Design and development of MoNbTaTiZr Porous High Entropy Alloys for Biomedical Applications

By

Muhammad Awais Munir Awan

School of Chemical and Materials Engineering (SCME)

National University of Sciences and Technology (NUST)

H-12 Islamabad, Pakistan

May, 2022

Design and development of MoNbTaTiZr Porous High Entropy Alloys for Biomedical Applications

Muhammad Awais Munir Awan

Reg No: 00000277163

This thesis is submitted as a partial fulfillment of the requirements for the degree of

MS (Materials and Surface Engineering)

Supervisor Name: Dr. Khurram Yaqoob

School of Chemical and Materials Engineering (SCME)

National University of Sciences and Technology (NUST)

H-12 Islamabad, Pakistan

May, 2022

DEDICATIONS

Dedicated to my beloved parents who are unparalleled in the entire world and my siblings.

ACKNOWLEDGEMENT

All glory to Almighty Allah for His countless blessings that enabled me to complete my research work and thesis.

I am thankful to my loving and caring family for their valuable prayers, support, recommendations, and encouragement. I am also grateful to my supervisor for his guidance and support.

Muhammad Awais Munir Awan

Reg No. 00000277163

Abstract

Titanium and Ti based alloys drawn significant attention than conventional counterparts (CoCr Mo, 316L SS) as orthopedic implant application due to suitable mechanical properties and sufficient chemical stability in physiological body environment. In the present study, b-type high entropy alloy MoNbTaTiZr with varying concentration of filler element was designed by thermo calc software and developed by arc melting route. 3D inter-connected porosity with porosity range (4.1,8.7,14 & 18%) was introduced with removal of filler element by novel chemical dealloying method. XRD and SEM results confirmed the formation of dual BCC microstructure. The elastic modulus and mechanical strength of implant are successfully optimized by synergetic effect of high entropy alloys and porosity. The elastic modulus tailored between (42- 3.5) GPa and yield strength between (803- 108.5) MPa respectively. The microhardness values are higher than bone. Interconnected open cell 3d porous structure enhance surface roughness, surface area and hydrophilicity thus enhance bioactivity. Metallic implants surface was alkali treated to enhance surface energy then coated with hydroxyapatite by biomimetic method to enhance bioactivity. Corrosion studies of high entropy foams were carried out in simulated body fluid at body physiological conditions. The developed foams show higher corrosion resistance and electrochemical stability, required for biomedical applications. Overall developed high entropy foams consist of biocompatible elements, shows superior mechanical properties then conventional materials used and are best suited material for orthopedic implants.

Table of Contents

Table of Figures

List of Tables

Chapter 1

1 Introduction

With increasing in aging population especially in the developed countries the older people who cross the age of forty are more likely to develop diseases like arthritis and joint discomfort, resulting in a surge in demand for artificial instruments made of biomedical materials to replace malfunctioning hard tissues. Intravascular stents, heart valves, cardiac simulators, and replacement implants in knees, hips, elbows, shoulders, ears, and dental are all examples of biomedical materials that can be employed in various sections of the human body. Among them implants employed to replace the knees, hips and shoulders joints required special consideration because osteoarthritis (that is inflammation of the bone joints), osteoporosis (which is weakening of the bone), and trauma can cause discomfort or loss of tissue function, so implants used for hip and knee joint replacements have a lot of requirements. Implants defined as "biomedical devices which made of natural or artificial materials used to replace the lost biological structure, diseased structure and enhance the life quality"[1, 2].

Figure 1-1 Biomedical implants for hip and knee replacement

According to research, only in USA the number of hip replacement surgery increases by 174% and knee replacement by 673% from the present rate till 2030[3]. The rise in joint replacement surgery can be attributed to an increase in both replacement and revision surgeries. The revision surgery is defined as “failure of implant and have to remove, so for that purpose surgery is perform known as revision surgery”. The stress shielding effect, debris generation, foreign body response and release of ions from the implant in the host body are the main causes which results in failure of implant. So, there are some desired properties which are expected an implant should have. For hip and knee replacement, the implant should have good mechanical strength, high corrosion and wear resistance, excellent bio compatibility, and is nontoxic for body.

1.1 Classification of implant materials

Implant materials are divided into several categories.

- Ceramic implants
- Polymeric implants
- Metallic implants

1.1.1 Ceramic implants:

Ceramic materials implant has very good biocompatibility, high hardness and wear resistance, and produce least wear debris in the physiochemical environment. Ceramic implants have generally three types which is categorize as bioinert, bio-degradable and bioactive. Although ceramic implants have high biological properties but these material lake in mechanical properties. These materials have very low fatigue strength and high elastic modulus which is highly non-desirable in bio-implant applications[4-7].

1.1.2 Polymeric implants:

Polymeric implants have also good biocompatibility. Generally polymeric materials used in the variety of tissues including cardiovascular, neural, musculoskeletal, and cutaneous. In long term application these materials generally cause adverse effect by releasing the debris in the body due to lower wear resistance. Also, for hip, knee, and

dental application these materials are not suitable because of their low mechanical properties[8].

1.1.3 Metallic implants:

Metallic implants are the mostly used in the hip, knee, and dental application in which compatible mechanical properties are first priority. Although metallic implants have lower biocompatibility as compared to polymeric and ceramic implants but for long term application metallic implants are used due to a large number of flexible options. The possibility of modification or alteration of biological and mechanical properties according to requirement of application make them most suitable option compared to the other materials.

Therefore, metallic implants are mostly employed in load bearing applications and market share of metallic implant increases with time.

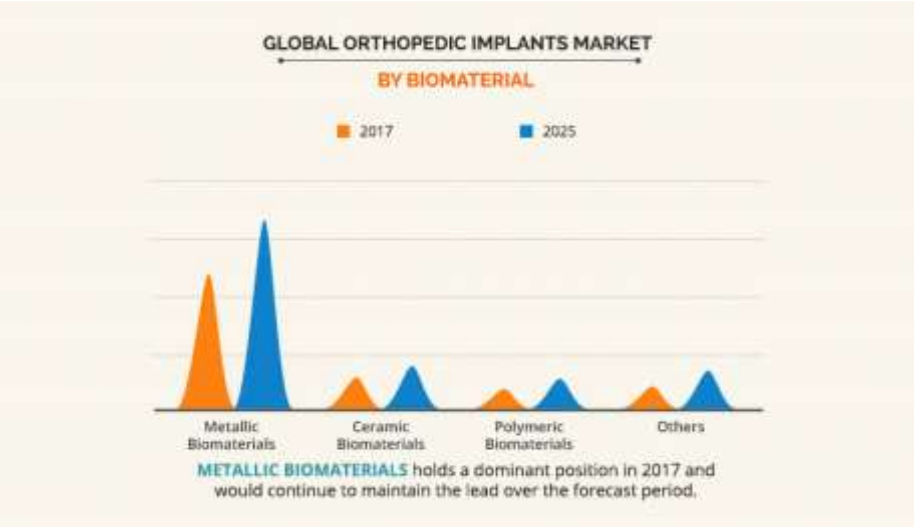

Figure 1-2 Market share of different classes of biomaterials

As discussed above the metallic implants have some shortcomings which have to be addressed to avoid the failure of implants in future and cause the revision surgery which is unfortunately very painful and have less chances of success as compared to first surgery.

1.2 Issues in metallic implants:

The main issues related to metallic implants are

- ❖ High elastic modulus
- ❖ Lower biocompatibility and poor fixation

1.2.1 Higher elastic modulus

Metallic implants have higher fatigue strength then other materials used. Also, they have good mechanical strength which make them capable and desirable material for load bearing applications, but metallic implants have high modulus as compared to the bone. If the implant has higher modulus compared to replaced or diseased bone, then the stress shielding effect occur which results in failure of implant. Higher modulus of implant prevents the uniformly distribution of necessary stress to the adjacent bone which results in weakening newly formed bone, the bone resorption happening and results in bone cells death[9-11].

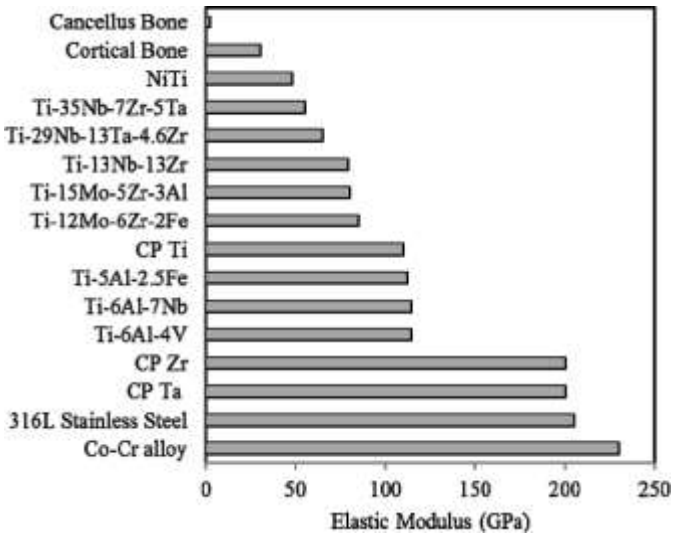

Figure 1-3 Comparison of elastic modulus between various metallic materials used [12]

In the above diagram the difference in modulus between the bone and the used metallic implants are given from which we can clearly see the large difference in moduli that cause the stress shielding effect and results in failure of implant and damage of bone.

1.2.2 Low biocompatibility and poor fixation

After the placement of implant in the body a chain of biological reactions occurs on the surface of the implant and surrounding body environment. Due to the stable nature of metallic implants, they are unable to produce good bonding with the adjacent bone. A layer of fibrous tissues covered the implants surface and isolate it from the surroundings which impede the necessary proteins, cells, and enzymes to reach the implant surface and grow. So due to isolation and low bioactivity of metallic implants healing time increases and micro movements occur as a result of a lack of strong bonding between the bone and the implant, causing excruciating discomfort.

1.3 Efforts made to resolve the issues pertaining to metallic implants

1.3.1 Reduction in elastic modulus

1.3.1.1 Beta type alloys

As discussed above the main problems with the metallic implants are higher elastic modulus. The potential solution of these short comings is to design and develop the lower modulus β-type implants because β-type alloys possess lower modulus as compared to the α-type and (α + β)-type alloys[13-15]. To make single β-type metallic implant β stabilizer elements (Mo, Nb, Ta etc.) added in the alloy.

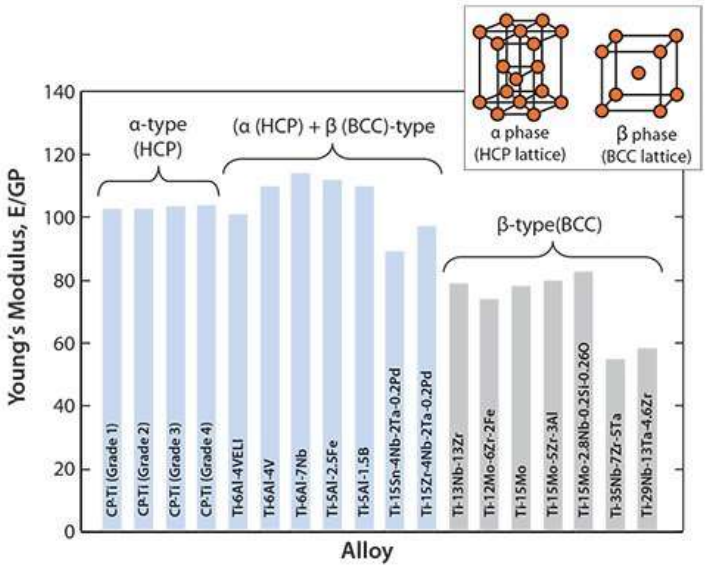

Figure 1-4 Comparison of mechanical properties between α, (α + β) and β-type titanium materials

1.3.1.2 Porous implants

The modulus decreases by making single phase β-type alloys, but the problem is that the beta type metallic implants still have higher modulus then the bone (10-30 GPa). So, introduction of porosity is the most popular solution to alter the elastic modulus according to the desired application[16-19]. By making porous implants stress shielding effect can by reducing the elastic modulus. Also, with the introduction of porosity surface roughness enhanced and more sites are available for bone integration.

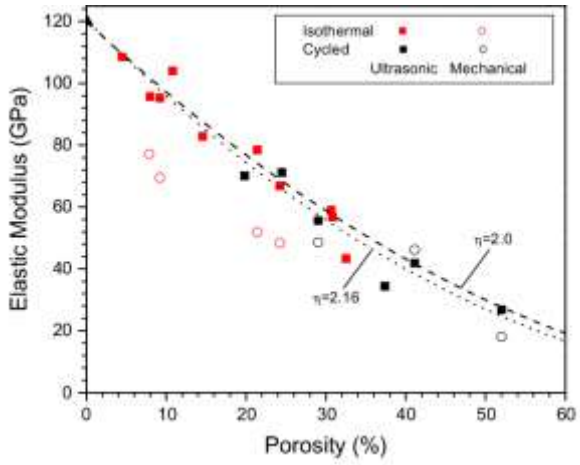

Figure 1-5 Elastic modulus as function of increasing porosity[20]

1.3.2 Surface modification

The second problem associated with the metallic implants are its low surface bioactivity and poor fixation. To fix this problem the surface of the implant is modified by chemical and physical treatments.

The physical treatments involve the increase in surface roughness, introduction of porosity and by grow nanostructures on the implant surface. As far as chemical treatments are concerned, bioactive coatings and alkali treatments are performed to enhance surface energy and bioactivity.

To fix this problem surface roughness enhanced by introduce the porosity which we were also done to decrease the elastic modulus. Further we were also performed chemical treatments and coatings to enhance the biocompatibility and surface activity.

1.3.2.1 Hydroxyapatite coating

After the placement of implant in the body the main concern is the integration between implant surface and the bone. Also, a number of chemical reactions occur on the surface of implant. Lower biocompatibility of the implant surface impedes the fixation of implant with bone which increase the healing time and in severe cases cause failure of implant. And if the implant surface has low chemical stability in the harsh body environment, it released toxic elements that cause harmful effects for health. To cop these problems hydroxyapatite coating on the implant surface is formed before the placement in the body. The hydroxyapatite is inorganic component of the bone which enhance the bonding between implant and bone and aid in osseointegration[21]. The HA coating on the implant surface mimic the natural bone and reduce the healing time. Also, the HA coating decreases the direct contact of implant surface and body fluids which helps the implant surface to retain its chemical stability.

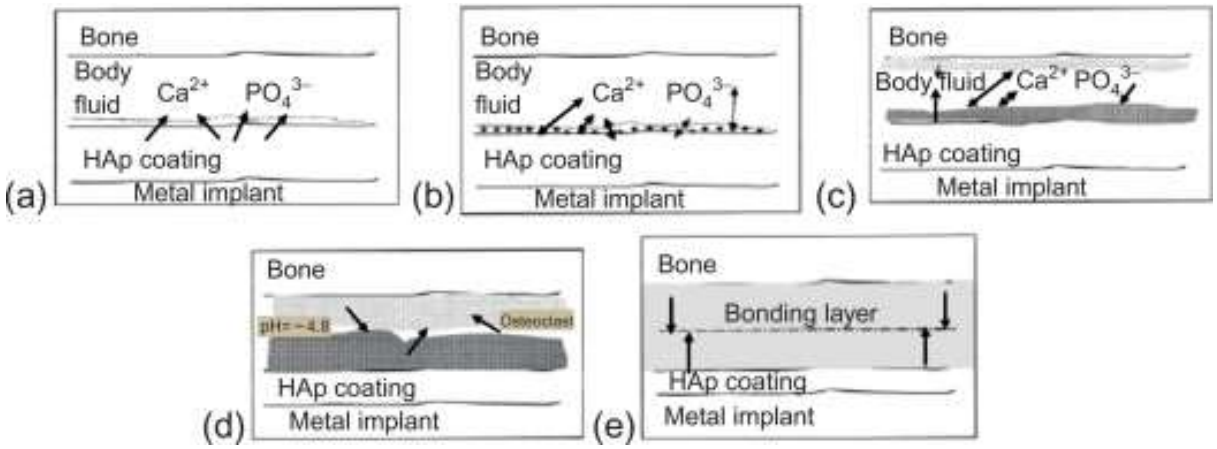

Figure 1-6 Improvement in implant bonding through HA coating once in vivo [22]

1.3.2.2 Alkali treatment

Alkali treatment is a chemical surface treatment process which results in growth of sodium or calcium titanate layer on the implant surface. The resultant modified layer enhanced the surface area and surface energy which leads to early growth of HA on the implant surface in the body environment and results in fast healing. Also, it improved matrix protein absorption, cell adhesion and proliferation, and, ultimately, better implant-bone osteointegration.

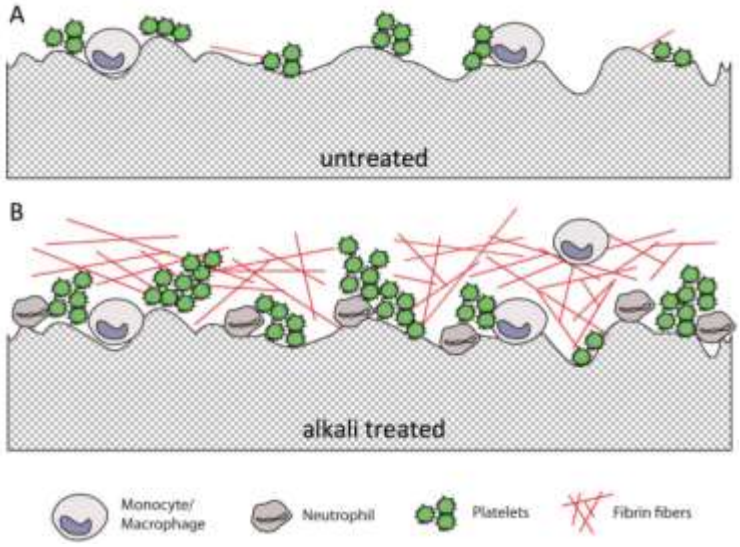

Figure 1-7 Difference in alkali treated and untreated samples by blood clots growth [23]

1.4 Metallic implants classification

Based on above discussion, metals and alloys are generally employed in the applications in which mechanical properties are a priority such as in load bearing applications. The metallic implants which are used for these applications are 316L stainless steel, Co-Cr alloys, Ti and Ti based alloys. Stainless steel and Co-Cr alloys have very high elastic modulus then the living bone. In contrary Ti and its alloys have lower elastic modulus then the counterparts.

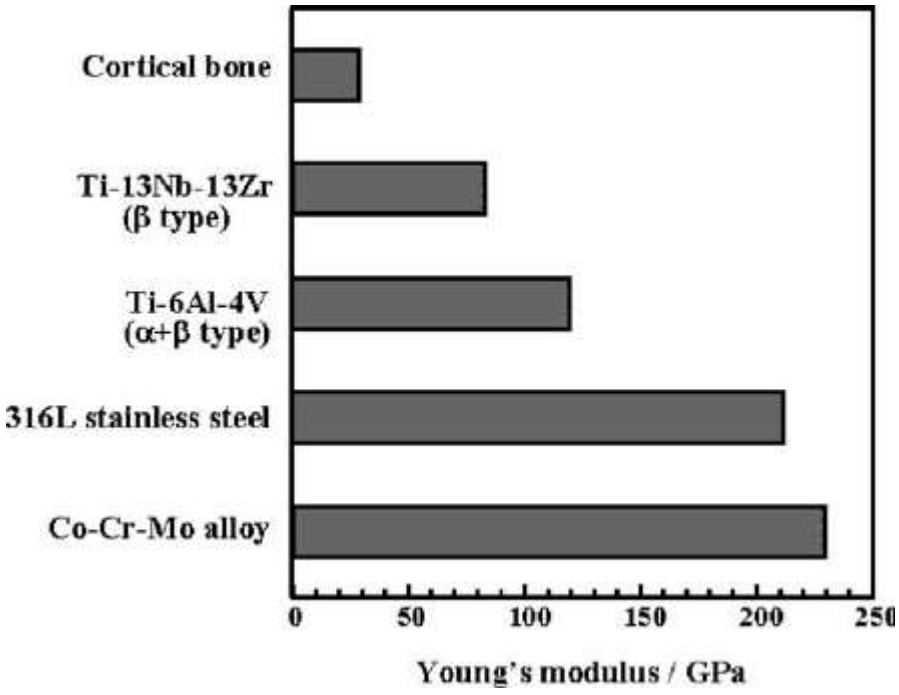

Figure 1-8 Elastic modulus comparison of metallic implants with bone [24]

The graph represents the modulus values of metals and alloys employed as biomedical implant. It is clearly visible titanium and titanium alloys have low modulus as compared to the other metallic implants. Also, 316L stainless steel and Co-Cr alloys are not chemically stable in body environment and loss toxic elements in the body. As comparison titanium remain chemically stable in the body environment which make titanium and its alloys more favorable metallic implants. That's why the demand of titanium and titanium alloys increases with time.

1.5 Chosen alloy

Titanium and its alloys have lower elastic modulus and chemical stability in body environment then other metallic implants. But still titanium and Ti alloys have high modulus compared to the living bone as shown in the graph above. So, we design MoNbTaTiZr high entropy alloy consist of five metals present in equiatomic ratio. Metals are carefully selected which are defined as biocompatible and non-toxic and do not produce any allergic reaction in the body. Selected metals Mo, Nb and Ta are beta stabilizer while the Ta is neutral in nature which helps to stabilize the single beta phase and results in lower the modulus. Also, to further decrease the elastic modulus to make it comparable to the modulus of living bone we introduced the porosity in different ratios.

1.6 High entropy alloy

Conventional alloys consist of two or sometimes three elements which limits the compositional space to design and develop new alloys with better properties. The development of multi-component high-entropy alloys (HEAs) has shattered the old design strategy.

High entropy alloys are defined as “High-entropy alloy is a multiple component alloy system containing five or more than five elements having concentration between (5-35%)[25-27]. Because of the direct increase in mixing entropy as the number of components of the system grows, multi principal systems are referred to be high entropy alloys. Entropy is a measure of a system's unpredictability and is made up of four basic components: configurational, vibrational, magnetic dipole, and electronic randomness. But in the case of high entropy alloys the main factor is configurational entropy because as the number of elements increases in a system then the number of ways increases of their arrangement in lattice. In terms of configurational entropy, HEAs are defined as those alloys which have configurational entropy higher than 1.5 R. The high entropy alloy (HEA) concept is a recent groundbreaking development in materials science that has allowed us to break free from material design constraints and reach a realm of apparently limitless possibilities. High entropy alloys have four characteristic effects which are

- ❖ High-Entropy effect
- ❖ Severe lattice distortion effect
- ❖ Sluggish diffusion effect
- ❖ Cocktail effect

$$\Delta G_{mix} = \Delta H_{mix} - T\Delta S_{mix}$$

1.6.1 High entropy effect

The high entropy effect of HEAs is the first and most important effect because it tends to stabilize the solid solution phase instead of intermetallic when five or more than five elements combine in equiatomic or near equiatomic ratio. According to physical metallurgy calculations when such large number of elements combine then the only phase has to form is intermetallic phase due to high entropy of mixing. But Gibbs energy equation suggests that when numerous numbers of elements combine then due to high configurational entropy value the only phase stabilize which has lower Gibbs free energy even the possibility of formation of numerous phases exist.

Here ΔG_{mix} is Gibbs free energy, ΔH_{mix} is enthalpy of mixing and ΔS_{mix} is configurational entropy where T is temperature.

The high entropy effect becomes more prominent at elevated temperatures.

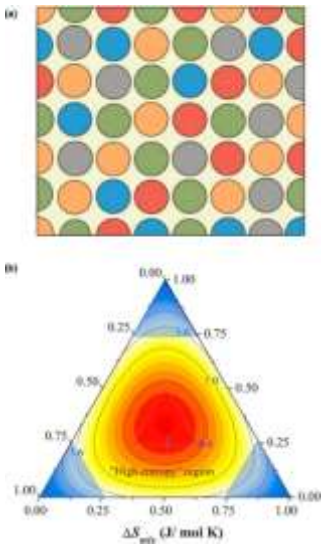

Figure 1-9 Pictorial representation of high entropy effect in HEAs [28]

1.6.2 Severe lattice distortion effect

Due to atomic radii difference between constituent elements, substantial lattice distortion occurs in high-entropy alloys. Due to severe lattice distortion in high entropy alloys as compared to the conventional alloys, a very large increase in configurational entropy is observed which reduce the intensity of XRD peaks to enhance the hardness, decreases the thermal and electrical conductivity and lessen the temperature dependence of these properties.” In case of high entropy alloys, the terms of "solvent" and "solute" are difficult to be defined in the traditional sense. The lattice distortion arises in high entropy alloys due to the presence of atoms of different radii having different types of bonding between them. The characteristics as well as the microstructure of high entropy alloys are affected by such lattice distortion.”

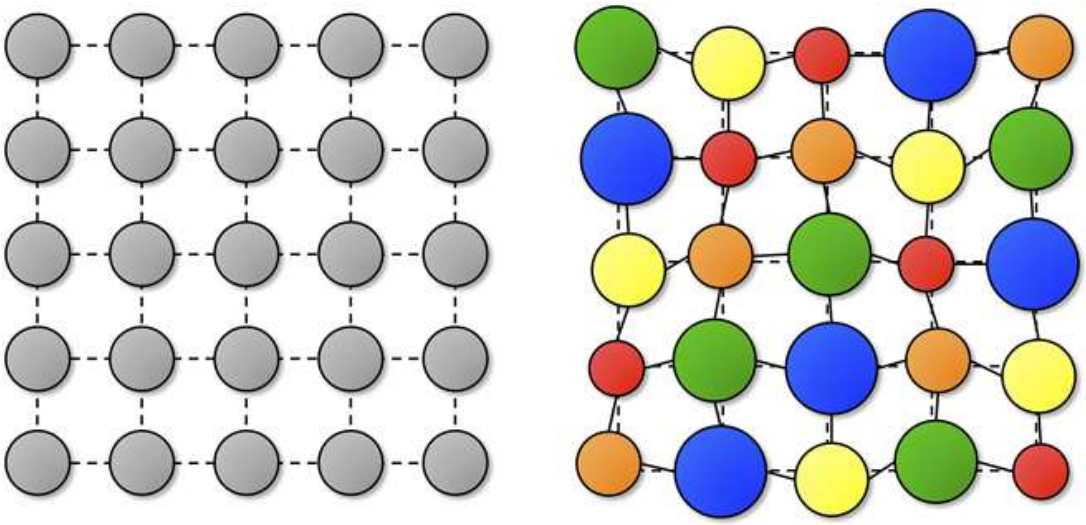

Figure 1-10 Pictorial representation of Lattice distortion effect in HEAs [29]

1.6.3 Sluggish diffusion effect

In contrast to typical alloys, where the primary element is the solvent and the element in lesser proportion is called the solute, a multicomponent system is regarded a whole-solute matrix. That’s why the diffusion phenomena are different in both types of alloys. During the creation of a new phase in HEAs, cooperation of atoms of principle elements is necessary. Sluggish diffusion in HEAs decreases phase conversion rates”.

1.6.4 The cocktail effects

The inclusive effect that develops as a result of interactions between constituent elements is known as the ‘cocktail' effect of high entropy alloys, when the amount of composing material present exceeds the average quantity predicted by the mixture rule. The ‘cocktail' effect serves as a reminder that when uncommon combinations of components and microstructures are mixed in a wide space of HEAs, unexpected outcomes might occur.

1.7 Research objective

The following are the aims of this study:

- Design the single beta-type high entropy alloy through Thermo Calc software which consist of non-toxic and bioactive elements.
- Development of designed high entropy alloy through vacuum arc melting route.
- Characterization of the developed alloys by using the XRD (x-ray diffraction), SEM (Scanning electron microscope) and EDS (Energy Dispersive Spectroscopy)
- High entropy foams of as-cast samples formed by removing the filler element through dealloying process.
- Characterization of developed foams in various percentage of porosity (0-20%) by using XRD (x-ray diffraction), SEM (Scanning electron microscope) and EDS (Energy Dispersive Spectroscopy), AFM (atomic force microscopy), DCA (contact angle)
- Mechanical properties of the developed foams study by mechanical characterization e.g compression and hardness testing
- To study the chemical stability of the developed alloy corrosion testing performed, OCP (open circuit potential), LRP (linear polarization resistance), EIS (electrochemical impedance spectroscopy), Potentio-dynamic polarization resistance.
- Surface modifications of the developed foams by HA coating and Alkali treatment to enhance bioactivity.

Chapter 2

2 Literature Review

2.1 Conventional biomedical implants for orthopedic applications

Biomedical implants are used to replace and perform the function of damage organ of host body. The first and foremost requirement of implant is its sufficient biocompatibility in the host body[30]. The chemical, physical, and biological characteristics of a biomaterial determine its efficiency. Mechanical characteristics such as high mechanical strength, comparable modulus, and appropriate toughness are required. In a physiochemical environment of the body, high corrosion resistance and biocompatibility are essential for success of implant. Polymeric, metallic, and ceramic materials, or a combination of these elements, are the most prominent materials used in implants. Metallic implants are mostly employed for orthopedic applications due to more compatible mechanical properties as compared to ceramic and polymeric implants. Although biocompatibility of metallic implants is limited then ceramic and polymeric counterparts, but this problem can be resolved by different surface treatments. Stainless steel, CoCrMo, titanium and its alloys are generally employed as biomedical metallic implants.

2.1.1 **Stainless steel**

The first practical effort at a metallic implant material was 316L stainless steel. The stainless steel 316L is the most widely used implant material due to its high strength, ease of fabrication and relatively cheap cost[31]. Stainless steel has some drawbacks which make it un-desirable for long term implant application. The SS 316L have very high elastic modulus as compared to bone which cause stress shielding effect[4, 32]. The corrosion resistance is reasonable but for long term usage in body environment the release of Ni and Cr ions observed which cause allergic reactions[33]. Inflammatory and immunological reactions in the human body might be triggered by the release of these toxic ions. High elastic modulus and corrosion has been recognized as the leading cause of 316L implant

removals. That classified SS 316L alloys as having a lower level of biocompatibility than CoCrMo, Ti and Ti alloys.

2.1.2 CoCr Mo alloy

The CoCr MO alloy have high strength**,** good corrosion resistance as compared to SS 316L. The elastic modulus of CoCr MO alloy is very high then the bone which can cause stress shielding effect leads to failure of implant[34, 35]. The creation of a passive Cr_2O_3 layer immediately on the surface of the CoCr Mo alloy after placed in the body is considered to contribute to its high corrosion resistance[36]. Despite the fact that the spontaneous creation of a passive coating shields the CoCr Mo alloy's surface from reacting with the surrounding environment, wear debris can cause abrasion of this coating, which can reduce its protective capabilities, especially in hip and knee joint applications. Ions released by cobalt-chromium alloys have the potential to harm adjacent tissues. Cobalt is a carcinogen, and its release in the body stimulates cancer.

2.1.3 Titanium and Ti alloys

Titanium and its alloys are one of the latest categories of metallic biomaterials that has received a lot of attention and has proven rather prominent for application in biological environments[37, 38]. Ti has lower elastic modulus and high corrosion resistance then above discussed alloys. Because of its superior biocompatibility, titanium does not produce allergic reactions. Titanium does not release toxic ions in the body due to its stable passive layer in the body environment. Ti and its alloys are recognized as the extremely desirable preference for orthopedic implants due to their low density, high strength, high corrosion resistance, complete inertness to the physiological environment, excellent biocompatibility, low elastic modulus, and high capacity to join with bone and other tissues[1, 39]. Ti implants have some drawbacks. Generally, Ti implants have four grades, and all are α-type[40]. The modulus of titanium is lower than the SS 316L and CoCrMo alloys, but it is quite higher as compared to bone which can cause stress shielding effect. Also, the strength of pure Ti implants is considerably reduced at room temperature, and heat treatment is usually ineffective since the hcp structure seems to be very stable. The yield and ultimate tensile strengths of all four classes of CP–Ti are between 170 and 480

MPa and 240 and 550 MPa, respectively. Because of their low mechanical and fatigue strength, Ti implants cannot be employed in load-bearing applications.

2.1.3.1 Ti6Al4V alloy

Ti6Al4V is the most commonly employed titanium alloy for implant applications among the titanium alloys. Ti6Al4V is (α +β)-type Ti alloys and apart from CP–Ti, is the most frequently used biomedical alloy, accounting for 50% of total Ti production[41]. Ti6Al4V has a lower elastic modulus than 316 L and CoCr Mo alloys, which helps to prevent bone resorption caused by stress shielding. Also, it has high corrosion resistance, but it releases Al and V ions in the body when used for long term applications. Both ions are toxic for body and cause harmful effects such as Al ions cause Alzheimer's disease and V ions are classified as hazardous substances because of their significant potential for cytotoxicity[1, 12, 42, 43]. Due to toxic effect a number of (α +β)-type Ti alloys were produce for biomedical applications such as CP–Ti, Ti–6Al–4V, Ti–6Al–4V ELI, Ti–6Al–7Nb, and Ti–5Al–2.5Fe, but these all alloys still have both or one toxic element and their high elastic modulus describe that (α + β)-type Ti alloys are not best choice for biomedical implants. These considerations prompted the development of β-type Ti alloys with non-toxic β-stabilizers (such as Mo, Nb, Ta, and Zr) having lower elastic modulus and improved biocompatibility.

2.2 High entropy alloys

Due to above mentioned limitations researchers have endeavored to investigate innovative materials in order to find a suitable replacement for traditional metallic biomaterials. Due to limited space available in the design and development of binary and ternary alloys to achieve desirable properties, a new type of multicomponent alloys named as high entropy alloy was design and developed in 2004[25]. Due to its improved physical and mechanical characteristics, high-entropy alloys (HEAs), a novel form of metallic material with equimolar or non-equimolar compositions, have attracted interest. As compared to the conventional metallic alloys, high entropy alloys consist of more than four elements with varying concentration between 5-35%[44]. Right after their discovery in 2004, a huge number of high entropy alloys were formed till date. Among all those HEA’s only alloys

consist of non-toxic β stabilizer refractory metals such as Mo, Nb, Ta, Ti, Zr, Hf, are desirable candidate as biomedical implants. One of the most typical characteristics of RHEAs made up of these elements is that the BCC phase can occur in many of them, and even a single BCC phase's lattice structure can be seen. Along with BCC phase these high entropy alloys have high hardness and mechanical strength due to significant lattice distortion effect resulting from the integration of different-sized component parts into a solid solution phase.

2.2.1 Four core effects of High entropy alloys

The exceptional qualities of high-entropy alloys are due to a number of factors[45]. The four core effects are the names for these contributions high-entropy effect; sluggish diffusion; severe lattice distortion; and cocktail effect.

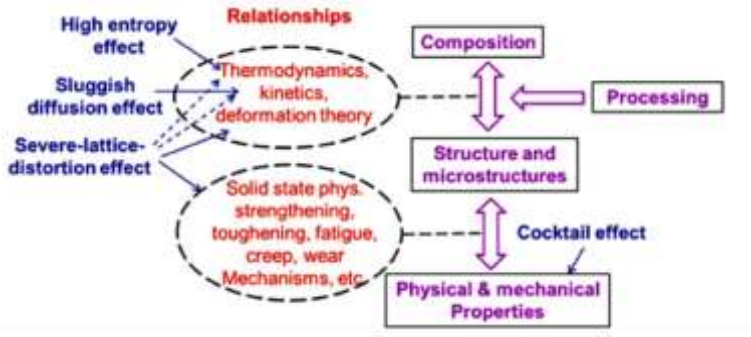

Figure 2-1 The four core effects in high entropy alloys**[46]**

2.2.1.1 High entropy effect

High entropy effect is defining as multi-principal elements have a large mixing entropy which results in their Gibbs free energy is lower, allowing random and partially ordered solid solutions to compete with intermetallic complexes for equilibrium states at high temperatures. Also, when there is a significant difference in enthalpy of mixing of constituent elements, the formation of more than two phases is more likely in high-entropy alloys appear.

2.2.1.2 Sluggish diffusion effect

Higher recrystallization temperatures and creep resistances, slower grain growth and particle coarsening, and ease of obtaining supersaturated states and fine precipitates are all caused by the sluggish diffusion effect, in which the number of fundamental components in the system's matrix is proportional to the degree of sluggish diffusion.

2.2.1.3 Lattice distortion effect

The atomic size difference parameter is also important here along with the entropy of mixing (ΔSmix) and the enthalpy of mixing (ΔHmix) when defining trends and determining phase selection rules. A significant solution hardening effect is often caused by a severe lattice distortion effect, in which various atomic sizes, bonding energies, and crystal structure tendencies among individual components all contribute to the lattice distortion. As a result of lattice distortion effect qualities such as strength and hardness are improved significantly, and the temperature dependence of these attributes is reduced.

2.2.1.4 Cocktail effect

The cocktail effect is defined as each phase, which is a multi-principal element solid solution, is treated as an atomic-scale and microscale composite, with multi-principal component composite effects and multiphase composite effects, accordingly.

2.3 Comparison of properties between conventional and high entropy implants

2.3.1 Comparison of mechanical properties between conventional and high entropy implants

2.3.1.1 Conventional implants

As discussed above right after their discovery in 2004, a huge number of high entropy alloys were designed and developed, but in case of biomedical applications we emphasize only on the HEA’s which consist of non-toxic and β stabilizers elements generally consist of refractory metals. We discussed mechanical and chemical properties of RHEA’s developed for biomedical implant applications and compare with SS 316L, Ti and

Ti6Al4V. The SS 316L has elastic modulus in the range of 180-200 GPa that is quite high as compared to the modulus of bone 30GPa and cause stress shielding effect[47], the Yield strength is in the range of 172 to 160 MPa which is good for load bearing applications and tensile strength is lies in the range of 480 to 485 to 860 which is also good for biomedical applications. On the contrary Co based alloys which used for biomedical applications have elastic modulus in the range of 220 to 230 GPa which is higher than the modulus of SS 316L and became the one of the big reasons for failure of implant due to stress shielding effect[48]. Other mechanical properties of Co based alloys are excellent for load bearing applications, YS and TS are lies in the range of 450 to 1500 MPa and 655 to 1900 MPa respectively. On the other hand, Titanium implants has lower elastic modulus as compared to SS 316L and Co based alloys generally in the range of 100 to 115 GPa[40, 49]. Although Ti implants have considerably lower modulus, but it is still very high when compared to the modulus of bone and can cause stress shielding effect leads to failure of implants. The lower elastic modulus also effects the other mechanical properties of Ti implants which are essential for load bearing applications such as YS and UTS lies in the range of 170 to 480 MPa and 240 to 550 MPa respectively[50] which is quite lower then Co based implant materials. Now if we consider Ti6Al4V alloy, its elastic modulus lies in the range 101 to 115 GPa[51] which lower than SS 316L and Co based alloys, comparable with titanium implants and higher than the modulus of bone. Although Ti6Al4V has comparable modulus with the titanium implants, but its other mechanical properties are considerably higher than the titanium implants such as YS and UTS lies in the range of 795-869 MPa and 895 to 965 MPa which make it favorable as implant material than titanium[52], SS 316L and Co alloys in term of mechanical properties.

A general comparison in the light of above discussion about mechanical properties of conventional alloys can be represent in graphical form as,

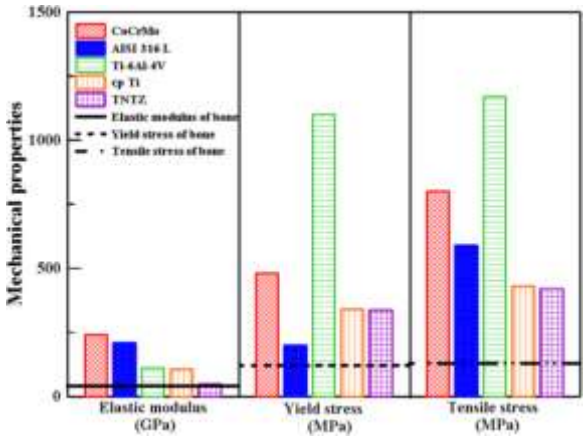

Figure 2-2 Graphical representation of mechanical properties of conventional materials for biomedical applications[53]

2.3.1.2 High entropy alloys

In case of high entropy alloys, we only discuss only those alloys which consist of no toxic elements for biomedical applications (Mo, Nb, Ti, Hf, Zr, Ta) and have BCC or (HCP+BCC) structure to achieve high strength and ductility, lower modulus, improved fracture resistance, and hardness, and so avoid difficulties caused by loss of bone integrity, which can result in an implant's unexpected failure, and mechanical insufficiencies over service life. By arc melting technique, Wang and Xu (2017) created a TiZrNbTaMo equiatomic HEA with BCC1 and BCC2 dual phases. This alloy shows elastic modulus of 153 GPa which is higher than the modulus of Ti, Ti6Al4V and bone but have very high YS 1390 MPa and low value of ductility[54]. Dirras et al. (2016) investigated the mechanical properties of as-cast TiHfZrTaNb HEA made by arc melting route which shows lower elastic modulus of 80GPa with 800 to 985 MPa YS[55, 56]. The TiZrHfNbTa HEAs were developed by Yuan et al. (2019) by arc melting route and study their mechanical properties, the elastic modulus of Ti25Zr25Nb25Ta25, Ti45Zr45Nb5Ta5, and Ti15Zr15Nb35Ta35 lies in the range of 57 to 89 GPa and their YS lies in the range of 728 to 1367 MPa[57]. Popescu et al. prepare TiNbTaZrFe high entropy alloy by powder metallurgy route which have lower modulus value of 52 GPa and YS is 2425MPa.

Equimolar TiZrHfNbTa have elastic modulus 103 GPa and YS 1200 MPa with 12% ductility. Equimolar TiNbZrTa have elastic modulus 89 GPa and YS is 970 MPa whereas

ductility is 23%. Also, $Ti_{6.3}Zr_{6.3}Nb_{6.3}Ta$, $Ti_7Zr_7Nb_5Ta$ and Ti_9Zr_9NbTa has elastic modulus 75, 69, 57 GPa respectively whereas YS values are 798, 780 and 690 MPa respectively. The ductility decreases accordingly 29, 26, 24% respectively.

Material	Condition	E (GPa)	Yield Strength (MPa)	Ductility (%)	Efficiency Function i (10^{-5})
Ti-6Al-4V (ELI) *	Mill annealed [25,33]	110	850–900	10–15	3.87
Equimolar TiZrNbTaMo	As-cast arc-melted [34]	153	1390 ± 75	$\varepsilon_p \approx 6$	4.75
$Ti_{1-4}Nb_{0-6}Ta_{0-6}Zr_{1-4}Mo_{0-6}$	Selective laser melting [32]	140 ± 9	1690 ± 78	$\varepsilon_t = 1.32 \pm 0.19$	8.50
Equimolar TiZrHfNbTa	As-cast arc-melting in a Ti-gettered high-purity Ar atmosphere [35]. Remelted at least 6 times to ensure chemical homogeneity	103	1200	12	8.42
TiZrNbTa (Alloy 1)		89	970	23	7.66
$Ti_{6-3}Zr_{6-3}Nb_{6-3}Ta$ (Alloy 2)		75	790	29	7.56
$Ti_7Zr_7Nb_5Ta$ (Alloy 3)		69	780	26	9.00
Ti_9Zr_9NbTa (Alloy 4)		57	690	24	11.29
$TiZrNbTa_{1-62}$ (Alloy 5)		93	1050	12.7	8.12
$TiZrNb_{2-33}Ta_{2-33}$ (Alloy 6)		135	970	12.5	3.03
$Ta_{0-7}HfZrTi$		77	1046	14.31	12.46
$Ta_{0-8}HfZrTi$		85	1120	4.63	11.35
$(TaNb)_{0-6}HfZrTi$		73	880	19	10.01

Figure 2-3 Some recently developed high entropy alloys for biomedical applications[58]

From the results we conclude that by increasing the Nb and Ta content the value of elastic modulus increases but other mechanical properties are also improved. We can decease the value of elastic modulus by increasing the Ti and Zr content in the alloy, but the value of ductility and YS also affected with modulus. But after a certain increase in Ta and Nb content the value of elastic modulus increases accordingly as we discussed above but the ductility sacrifice and decreases such as $TiZrNbTa_{1.62}$ and $TiZrNb_{2.33}Ta_{2.33}$ have elastic modulus 93 and 135 respectively having ductility 12.7 and 12.5%.

2.3.2 Comparison of electrochemical properties between conventional and high entropy alloys

Corrosion behavior of refractory high entropy alloys were also reported in the stimulated biological fluids at body and room temperatures and results were compared with 316L SS, CoCr Mo and Ti6Al4V alloys in the same conditions. Motallebzadeh et al. (2019) studied the corrosion behavior of TiZrTaHfNb and Ti1.5ZrTa0.5Hf0.5Nb0.5 high entropy alloys in phosphate buffer saline solution at 37C and named them as RHEA 1 and RHEA 2 and compare the results with 316L SS, CoCr Mo and Ti6Al4V alloys. Pitting corrosion observed on the surface of 316L SS, CoCr Mo and Ti6Al4V alloys after corrosion experiment, whereas no pitting observed on the surface of RHEA1 AND RHEA2 surface. With a continuous passive plateau up to 1800 mVAg/AgCl, high value of Ecorr and lower value of Icorr, RHEA1 and RHEA2 shows high chemical stability in the body environment conditions. The wettability by using sessile drop method were also measured which shows that RHEA1 and RHEA2 have similar wettability with Ti6Al4V, and higher hydrophilicity as compared to 316L SS and CoCrMo alloy. Wear resistance of RHEA1 and RHEA2 is also superior to 316L SS, CoCrMo and Ti6Al4V alloys[59]. Corrosion and wear resistance of equimolar MoNbTaTiZr HEA were also studied in simulated body fluid at room and body temperature and compare with SS 316L[60]. The results shows that MoNbTaTiZr HEA have higher corrosion and wear resistance than 316L SS at both room and body temperature. M. Akmal et al. (2021) study the corrosion behavior of MoNbTaTiZr in PBS solution at room temperature and compare the results with 316L SS and pure Ti[61]. The results revealed that MoNbTaTiZr high entropy alloy have high corrosion resistance than SS 316L and comparable with pure Ti. The SS 316L shows pitting after 0.4V whereas Ti and MoNbTaTiZr show no sign of pitting even at 1.2V. G Popescu (2018) prepared TiZrNbTaFe high entropy alloy by powder metallurgy route, and its corrosion behavior was study in ringer lactate solution at 37^0C and compared with Ti6Al4V[62]. The corrosion results indicate that TiZrNbTaFe have higher corrosion resistance than Ti6Al4V. It is observed that addition of Nb and Ta significantly enhance the corrosion resistance where corrosion resistance also increases by increasing the Mo content in alloy.

From the results discussed above revealed that refractory high entropy alloys have superior mechanical and chemical properties than the conventional alloys generally employed for biomedical applications. Most of the refractory high entropy alloys have single phase BCC structure and have lower modulus than SS 316L and Co based alloys and comparable or generally lower than Ti and Ti6Al4V alloy whereas their other mechanical properties such as YS and UTS are considerably higher than Ti and Ti6Al4V and other conventional implants used for biomedical applications which make them more desirable for biomedical applications.

2.4 Efforts made to reduce the elastic modulus

Although the mechanical and chemical properties of high entropy alloys are better than the conventional implant materials, but their high elastic modulus and limited surface activity (inherent property of metallic materials) is yet required special attention to be addressed. Considerable efforts made to reduce the elastic modulus of implant materials to make it comparable with bone.

2.4.1 β-type alloys

Some of which are design β-type alloys because β-type alloys have lower modulus value than the α-type and (α + β)-type alloys. But problem associated with β-type alloys is that, have these alloys have lower elastic modulus but their YS and UTS are also reduced which is very important especially in load bearing applications. So as discussed above β-type high entropy alloys were developed which have lower elastic modulus with higher mechanical strength and chemical stability due to lattice distortion and sluggish diffusion effect.

2.4.2 Metallic foams

To further reduce the elastic modulus of metallic implants porosity is introduced. Porous Ti alloy structures have lower moduli than their bulky equivalents, in addition to producing low-modulus β -type Ti alloys as previously indicated. By making the porous implants we can adjust the value of modulus according to the application. Pore size and morphology can influence the mechanical characteristics of porous metal. Metallic foams are

biocompatible, have a larger elongation to failure, and have a low elastic modulus. By introducing the porosity, the surface roughness and wettability of metallic foam enhance which make it more biocompatible[63-65]. For biomedical applications open and connected porous channels are desirable. While increasing porosity, the porous metals may improve bone cell regeneration, but porous structures have the opposite effect on mechanical characteristics.

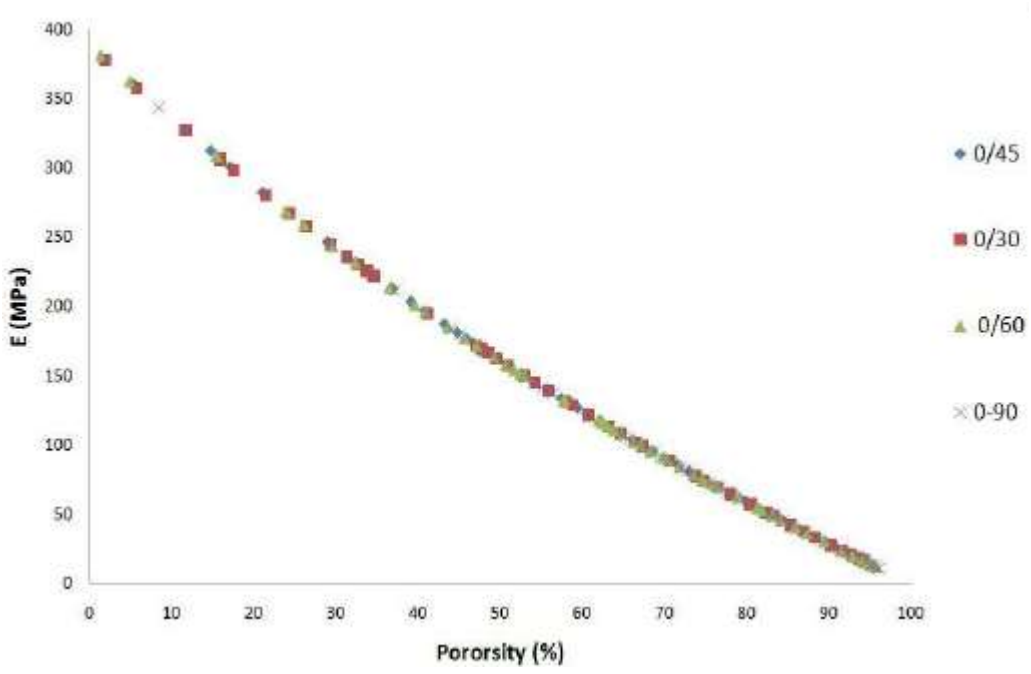

Figure 2-4 Effect of porosity on mechanical properties of metallic materials[66]

As a result, numerous preparation procedures for porous Ti alloys of appropriate strength have been investigated.

So, a number of methods were used to introduce porosity in metallic implants like space holder method[67, 68], rapid prototyping[69, 70], melt infiltration[71, 72], liquid metal dealloying etc but all these methods are lengthy, expensive, and required large number of parameters to consider before application. In this research we produce Ti foams by simple, easy, and low-cost chemical dealloying process which produce open pores which are connected to form porous channels. Some attributes of this process are

- Process takes place at room temperature

- ❖ No need of complex chemicals or parameters
- ❖ Time efficient (24 hours at max)
- ❖ Introduces open porosity and interconnectivity

The detail of novel chemical de-alloying process is discussed in chapter 3. By using this dealloying process porosity introduced from 1% to 20%.

2.5 Osseointegration

The ability of an implant material to join with natural bone is known as osseointegration. Ceramic and polymeric implants have high capability to integrate themselves with the living bone but due to the inadequate mechanical properties for load bearing applications cannot be desired for orthopedic applications. On contrary metallic implants have adjustable mechanical properties but lower surface activity and generally have inert nature in the body environment. The problems associated with the mechanical properties can be solved by formed the β -type porous refractory high entropy alloy. So, to enhance the biocompatibility different surface treatments of metallic implants are carried out. Right after placement of implant material number of biological and chemical reactions occur on the surface of implant, but due to inert nature of metallic implants it isolates itself from the surrounding and encapsulated by fibrous tissues which hinder the transport of vital cells and proteins to reach the surface of implant and in result implant cannot integrate directly with the deceased tissues, these phenomena enhance the healing time. So, a number of factors influence the osseointegration

- ❖ Surface roughness and surface area
- ❖ Wettability
- ❖ Surface energy

Higher surface area and surface roughness is desired for osseointegration. By introducing the porosity, the surface roughness enhanced significantly which promote the osseointegration. Also, the surface area enhanced by increasing the porosity, which can define as more area is available to living bone for integration.

For better osseointegration, the surface of implant material is hydrophilic. The introduction of porosity reduces the contact angle and enhance the wettability. The wettability can also be increased with increased in surface roughness and surface area and by application of some coating on implant surface which has hydrophilic nature.

Surface energy of metallic implant is lower which leads to inert behavior in the body environment. Surface can be enhanced by increasing surface roughness and by chemically activated the surface. Even if the surface is coated with some bioactive ceramic such as calcium phosphate, then there is possibility the coating is detached in the body environment due to low surface energy of metallic implant. So, to avoid this limitation the surface of the implant is chemically activated before ceramic coating.

2.5.1 Surface modification by hydroxyapatite coating

The most significant aspect of a biomedical alloy, after adjusting the mechanical properties according to bone by design the β -type high entropy alloy and addition of porosity, is to cover it with bioactive material to increase osseointegration and fixation. Hydroxyapatite is the non-organic part of the bone and consist of calcium and phosphate. Hydroxyapatite coating on implant surface carried out by different methods such as plasma spray, hydrothermal, sol-gel, electroplating and biomimetic method to enhance the surface bioactivity. With HA coating Infection based on biomaterials can be slowed, growth of fibrous tissue is minimized, foreign body response is avoided, cell proliferation will be amplified. Among all the HA coating methods biomimetic method is easy and can form uniform coating. This method is also work as biocompatibility test. The sample is cleaned ultrasonically with acetone, ethanol followed by water and then dried in air. Sample is dipped in simulated body fluid at 37^0C for 10 days.

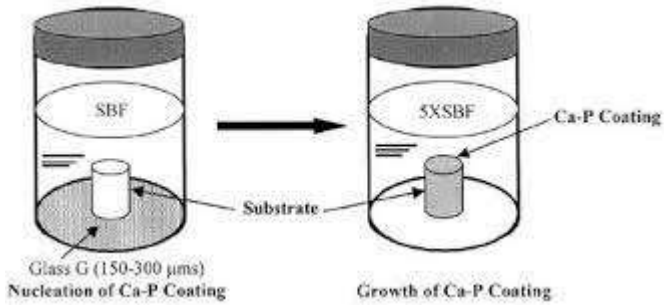

Figure 2-5 Sample immersion for bio-mimetic HA coating**[73]**

The solution changes after every 48 hours to maintain the pH. The simulated body fluid has the same concentration of ions as in the Human blood plasma. The pH of the solution is 7.4 which is same as for human blood. Different types of SBF solutions can be formed depend on the different concentration of ions of different constituents. Samples retrieve after 10 days and subsequently used for characterization after wash with deionized water.

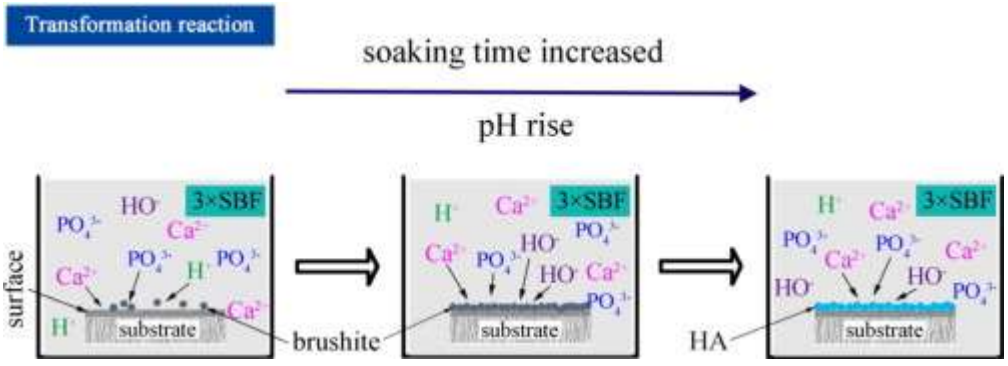

Figure 2-6 Schematic diagram of reactions occurs during biomimetic HA coating

2.5.2 Alkali treatment

Alkali treatment is chemical process to enhance the surface energy of the substrate. A simple chemical treatment in NaOH or Ca (OH)2 can prepare a bioactive titanium surface. At first titanium is leached in NaOH then the creation of a hydrated titanium oxide gel layer with alkali ions on its surface occurs. When this gel layer is dehydrated it form a layer of sodium titanate on the surface of titanium alloy. The alkali ions are released from this sodium titanate layer when this pre-treated titanium implant is exposed to SBF and in result hydronium ions enter in surface layer which form titanium oxide hydrogel layer on

surface. The released Na+ ions raise the pH of the soaking solution, increasing its degree of supersaturation with respect to apatite, and the titanium oxide hydrogel induces apatite formation on the titanium surface.

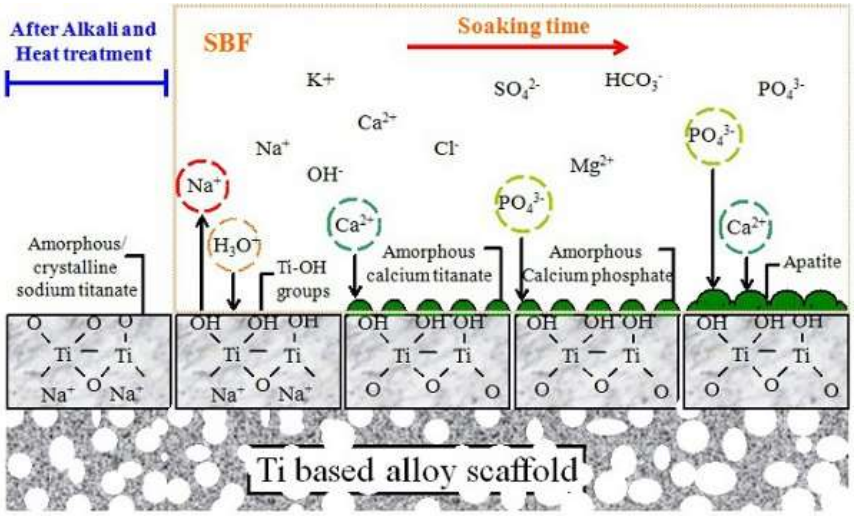

Figure 2-7 Hydroxyapatite growth on alkali treated metallic samples[74]

Samples were ultrasonically washed in ethanol and water for 5 minutes and dried in air. Samples were then dipped in 5M NaOH solution at 60C for 24 hours. After 24 hours washed with deionized water and dried at 100C. Sometimes samples were etched with HCl before immersion in solution to enhance surface roughness and increase the surface area.

Chapter 3

3 Experimental techniques

In the third chapter, experimental methods and characterization techniques are discussed. Designed alloys of different compositions were produced in arc suction melting furnace. After cutting the samples the samples through EDM wire cut microstructural characterization (SEM and XRD) of as cast samples were performed.

As cast samples were then de-alloyed and introduced porosity by removing the filler element. Microstructural (SEM and XRD), mechanical (hardness and compression), magnetic (MFM), and electrochemical (corrosion) characterization of de-alloyed samples were performed. De-alloyed samples were dipped in simulated body fluid for bio-mimetic coating. Also, to increase the osseointegration coating uniformity and strength, alkali treatment of de-alloyed were done and then soaked in simulated body fluid and compared the results. All steps involved from preparation of alloy till the complete characterization are described below.

- Alloy preparation
- Cutting through EDM wire cut
- Microstructural characterization
- De-alloying
- Microstructural characterization
- Mechanical testing
- Surface modification
- Electrochemical characterization

3.1 Preparation of Alloy

Designed alloys were prepared in arc suction melting furnace. Raw material used in alloy preparation were highly pure metallic chips.

Arc suction melting furnace have tungsten electrode and water-cooled copper hearth which have five crucibles in it. So, five alloys can be formed in single evacuation. Vacuum of 10^{-5} torr achieved in the chamber. After creating the vacuum in chamber argon gas inject in it. Copper hearth acts as anode while tungsten electrode acts as cathode. The schematic diagram and picture of used arc melting suction furnace used is shown in fig (3-1).

Figure 3-1 Vacuum arc suction melting furnace in SCME, NUST

Before melting of alloys titanium getter placed in hearth melt by applying the arc so that no oxygen left in the chamber. Then tungsten electrode placed on one of the crucible and metals chips placed in it acted as the counter electrode, as we apply the arc on it, large current passing through it and, in few seconds, melting take place. After the formation of alloy, it turned over with the assistance of tweezer without breaking the vacuum and remelted. The melting of alloy → solidification → 'turn over' → re-melting and again solidification, this process is typically repeated five times to achieved compositional homogeneity. Alloy of button shape was formed as shown in fig (3-2).

Figure 3-2 Button shape metallic sample formed in Vacuum arc suction melting furnace present in SCME, NUST.

These metallic buttons were then cut in desired shapes through EDM wire cut to perform further characterization.

3.1.1 Grinding and polishing

For metallographic analysis cut samples were mounted by using the Bakelite powder at the temperature 180^0C through mounting press present in SCME, NUST. Fig (3-3).

Figure 3-3 Mounting press machine present in SCME, NUST

Mounted samples were then grinded on standard grit sized silicon carbide emery papers from P400 to P2000. Subsequently these samples were then polished to achieve scratch free surface. Polishing of samples were done by using the alumina slurry (alumina powder size 0.5 micrometer) on polishing cloth. Afterward polished samples were washed thoroughly to remove the alumina residue from samples. Samples were then dried and placed in desiccator. Grinder and polishing machine used in this preparation are present in SCME, NUST. Fig (3-4).

Figure 3-4 Grinder and polishing machine in SCME, NUST

3.2 Characterization of samples

3.2.1 Scanning electron microscope

SEM analysis of prepared samples were performed. In SEM analysis a very fine beam of electrons focused on the test specimen surface due to which number of electrons and photons emit from the specimen surface and these knocked off electrons and photons focus on detector. The output from detector modulates the brightness of CRT (cathode ray tube). So, in result, a consequent point is plotted on cathode ray tube for every point of specimen on which electron beam focused. We used SEM analysis because sample preparation is easy for this, and we can get information about surface morphology, chemical composition, crystallography, and planes orientation. The schematic of SEM is shown in figure below fig (3-5).

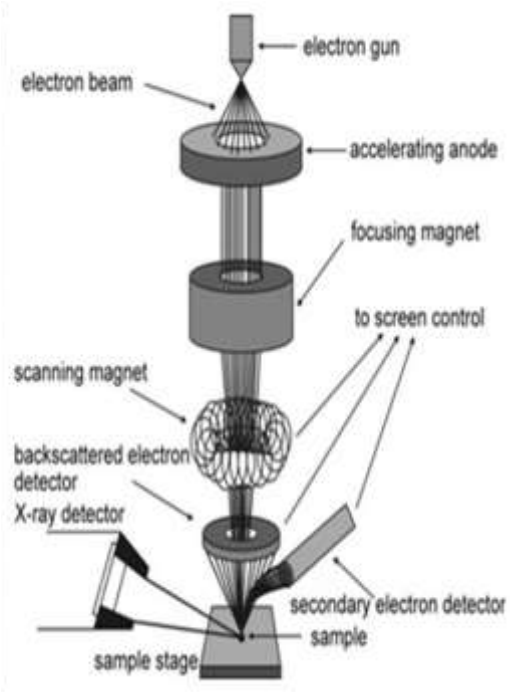

Figure 3-5 Schematic diagram of scanning electron microscope

SEM analysis was carried out by using the scanning electron microscope model (JEOL – JSM – 6490LA) present in SCME NUST and SEM model VEGA FESEM equipped with Bruker EDX at CASEN- NUST. The picture of SEM used in this study is given below fig

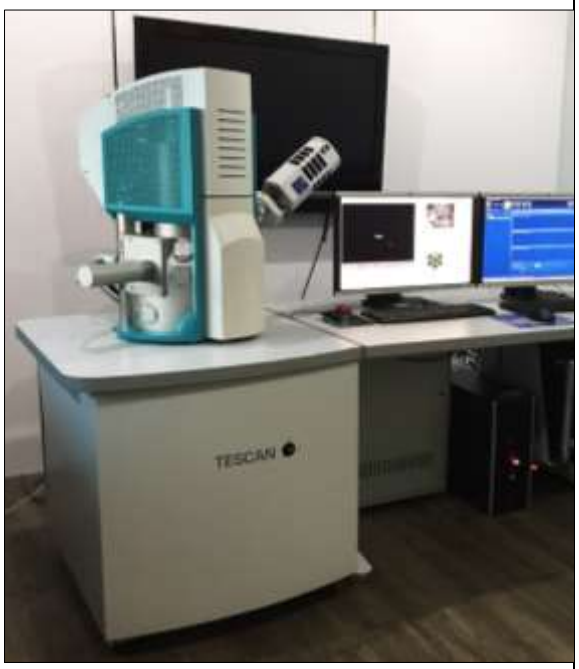

(a)	(b)

Figure 3-6 Scanning electron microscope equipped with EDS present in (a) SCME, NUST (b) USPCASE, NUST.

3.2.2 X-ray diffraction (XRD)

X-ray diffraction is a nondestructive technique used to study the different crystalline phases present in the test material. XRD consist of three parts cathode tube, sample holder and x-ray detector. Monochromatic electrons are generated by heating the filament in x-ray tube and accelerated towards the specimen. These electrons collide with the test specimen surface, reflect, and detected on x-ray detector. Crystal is composed of layers and planes. So, the x-rays which have wavelength similar to those planes reflect and constructive interference takes place which are accordance to Bragg's law (diffraction takes place when angle of incidence is equal to angle of reflection) and those "Bragg's reflections" picked up by the detector. XRD gives information about the phases and crystallinity. XRD schematic is shown in fig 3-7.

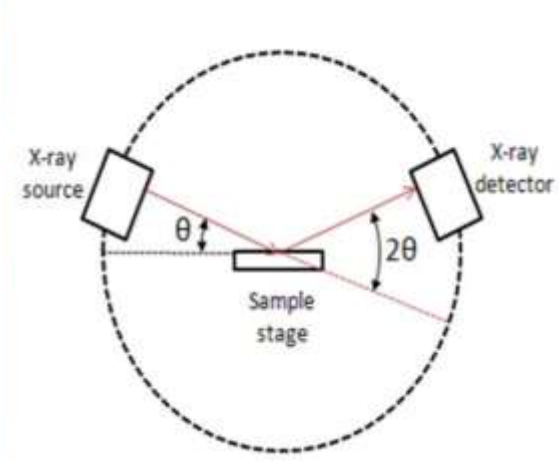

Figure 3-7 Schematic diagram of XRD

Samples were cut through EDM wire to ensure even geometry and in 2mm thickness. Samples were grinding and polished for XRD analysis. Even thickness of the sample will restrict the peak shifting due to uneven thickness of the samples. XRD used in this study is (D8, Advance Bruker) present in USPCASE, NUST.

De-alloying process

The process of de-alloying is using to introduce porosity by removing filler element to make metallic foam. The process of de-alloying comprises on simple steps

I. Weight of each alloy measured in weighing balance before dealloying.

II. Separate solution of 57ml deionized water and 3ml nitric acid (70% purity) prepared for each alloy in glass beakers. All the samples immersed in the solution for 24 hours and covered the beakers with parafilm. The time of immersion are note down.

III. After 24 hours samples will take out from the solution and washed with ethanol first and then with deionized water for 1 minute each.

IV. After washing samples will place on glass slides and dry on hot plate for 30 minutes at 130ºC.

V. The weight of samples measures again and calculate the mass loss.

Microstructural characterization of formed alloy was again carried out and compare the results before and after the de-alloying. Comparison of XRD results give information about the remove of filler element and SEM results comparison reveals the change in microstructure occurred after de-alloying process. Atomic force microscopy (AFM) was also carried out of foam samples to measure the surface roughness. Magnetic force microscopy (MFM) is mode present in AFM machine and MFM of the formed high entropy foams was also performed to find out the magnetic properties. AFM and MFM of the formed foams were performed on AFM (SPM) JSPM-5200 JEOL, JAPAN present in SCME, NUST.

3.2.3 Mechanical testing

3.2.3.1 Compression test

Compression testing of the test specimen performed to find out the materials response over compressive loadings. With the help of compression test we find a number of mechanical properties such as yield strength, young modulus, elastic limit, and compressive strength which are important to analyze whether the system we design have desired properties for

intended application or we have to design new system for that particular application. We perform compression testing because our ingot formed in furnace is too small for sample preparation for tensile test. So, we cut the button shaped alloy obtained from arc suction melting furnace through EDM wire cut into desired geometry according to the ASTM standard E9. The sample geometry for compression testing is shown in fig (3-8)

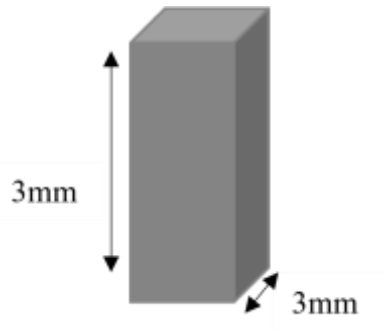

Figure 3-8 Sample geometry and dimensions for compression testing

We perform the compression testing on universal testing machine (UTM) SHIMADZU at SCME. As reported in literature, the strain rate set as 1×10^{-4} sec on UTM. However, during compression testing of such slender specimens the main hinderance occurred is known as buckling effect which define as “unstable lateral deformation of test specimen” and appears when the mating surfaces of the specimen are not perfectly flat. So, we prepare the sample by grinding and polishing and ensured the 100% flat surfaces. Also, carbide inserts were placed above and below the specimen to ensure the uniform distribution of force over cross-section surfaces as shown in fig 3-8.

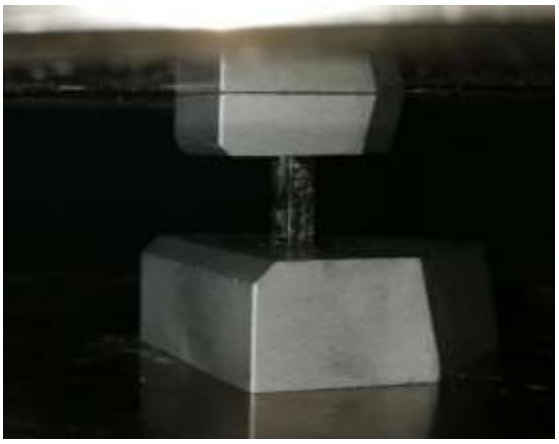

Figure 3-9 Carbide inserts placed above and below the compression samples

Three samples for each composition were prepared and tested, and average of results are used to describe the compressive strength. Fig 3-9.

Figure 3-10 Universal testing machine present in SCME, NUST

3.2.3.2 Microhardness test

Micro hardness tests were performed to measure the hardness or resistance to penetration of small or thin samples. Micro-Vickers hardness test was carried out on the polished mounted samples. In Vickers hardness test pyramid shaped diamond indenter is used to measure hardness of materials whereas Vickers hardness test is applicable to both micro and macro scales. Load up to 1000g is applied on indenter causes the plastic deformation in the surface of material. The shape of indentation is according to the shape of indenter. Vickers tests require accurate measurement from indent on the surface of material; these values are then put into the formula to calculate the hardness of materials. Micro hardness microscope is used to measure dimensions of indent because the size of indent is very small. Application of load for certain time produces indent in the sample, length of diagonal of indent is measure with the help of microscope. Putting the values of load and length of diagonals in the formula gives the hardness of materials.

Microhardness of the understudy high entropy foams were calculated by applying the load 100gf whereas dwell time was 15sec for indent. Indents were made on cell walls to calculate the microhardness of foams. A minimum of 12 indents were made on each sample to get average. Vickers hardness of both as cast and porous samples were carried out at same parameters for comparison.

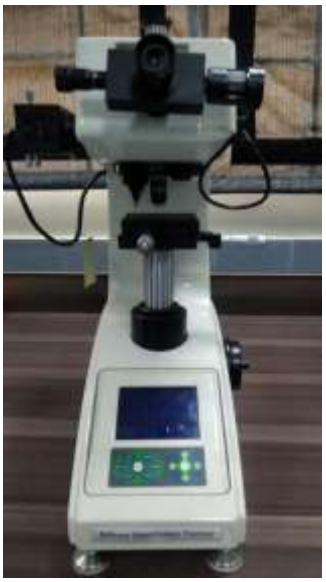

Figure 3-11 Micro-Vickers hardness tester at SCME, NUST.

3.2.4 Electrochemical characterization

Electrochemical characterization of the developed foams was carried out and results was compared with base metal alloy MoNbTaTiZr. Corrosion experiments were performed on Gamry workstation present in SCME, NUST. A three-electrode assembly was used for corrosion tests. Test specimen is used as working electrode having exposed surface area 0.2cm2. Platinum wire used as counter electrode and Ag/AgCl used as reference electrode. Tas SBF used as electrolyte having pH 7.4 and corrosion experiment perform at 37^0C. Open circuit potential (OCP) measures for 3600 sec, linear polarization resistance was performed from -10mVocp to 10mVocp at the scan rate of 0.166mV/s. Electrochemical impedance spectroscopy was performed from 100000Hz to 0.01Hz with an amplitude of ±10 mV. The equivalent circuit was design according to the system and formed in Gamry software and impedance data was analyzed by fitted with the designed equivalent circuit. Potentiodynamic polarization were also performed from -1500mVocp towards the 3000mVocp in anodic direction at a scan rate of 2mV/s. The values of corrosion potential and corrosion current density extracted from Tafel slope extrapolation. Gamry workstation Interface 1010E present in SCME, NUST used for electrochemical characterization.

3.3 Surface modification of High entropy foams

Surface modification of the formed foams were carried out to enhance the biocompatibility.

- Bio-mimetic coating of hydroxyapatite on high entropy foams
- Alkali treatment of foams

3.3.1 Bio-mimetic coating of hydroxyapatite

The surface of high entropy foams was modified with hydroxyapatite coating to increase the biocompatibility. For this purpose, bio-mimetic coating was done. SBF was formed by the Tas method because Tas SBF solution have ion concentration near to the human blood plasma. A comparison of ion concentration of Tas solution and human blood plasma are given in table below.

Table 1 Ionic concentration of Tas Sbf vs Human blood plasma

Formulation	**Na^+**	**K^+**	**Mg^{2+}**	**Ca^{2+}**	**Cl^-**	**HCO_3^-**	**HPO_4^{2-}**	**SO_4^{2-}**	**Buffer**
Blood Plasma	142.0	5.0	1.5	2.5	103.0	27.0	1.0	0.5	
Tas-Sbf	142.0	5.0	1.5	2.5	125.0	27.0	1.0	0.5	Tris

NaCl, NaHCO3, KCl, Na2HPO4.2H2O, MgCl2.6H2O, Na2SO4, (CH2OH)3CNH2, CaCl2.2H2O and HCl was used to prepare the simulated body fluid (Tas). We got 700ml of de-ionized water and the above-mentioned chemicals dissolved in water in appropriate quantity one by one after the first added chemical dissolve completely. A total of 40 ml of HCL 1 M solution was used for pH adjustment.

Just after the addition of fifth chemical 15ml of HCl solution was added and the remaining 25ml of HCL solution was added during titration process. After the addition of 8^{th}

chemical, the temperature of solution was raised from room temperature to 37C and then titration of solution carried out. During titration process consecutively water was added in the solution till the volume of the solution become 1 liter.

The developed foams were soaked in simulated body fluid and placed in an incubator at 37C for a period of 10 days. The solution was replaced with fresh solution after every two days to maintain the pH of the solution. After 10 days the samples were collected and rinsed with de-ionized water and dried in air. For the characterization of HA coated samples XRD, SEM, FTIR and contact angle were performed. Also, the weight of foams before and after the HA coating was measured for gravimetric analysis.

3.3.2 Alkali treatment for biomedical application

Surface of the developed foams were also modified by alkali treatment before the bio-mimetic coating. SEM of the alkali treated samples were carried out to find out changes on foams surface. Wettability of the surface checked by contact angle measurement. Alkali treated samples were then dipped in simulated body fluid to find out the effect of alkali treatment on mineralization of bone during in vitro study. In alkali treatment, polished samples were ultrasonically clean in acetone, ethanol, and water for fifteen minutes each and dried in air. These samples were then dipped in 100ml of 5M NaOH solution for 24 hours at 60C in an oven, then wash with water and dried in air.

The weight of foams was measured before and after the alkali treatment because we measure the HCA formation on alkali treated and without alkali treated samples with gravimetric analysis. The increase in sample weight is an indication of hydroxyapatite layer formation. SEM, FTIR and contact angle were performed again to study the coating surface characteristics and hydrophilicity.

Chapter 4

4 Results and discussion

The main objective of this research is to develop high entropy foams for biomedical applications, which have low elastic modulus comparable with the human bone and have high biocompatibility. So, in the previous section we discussed about various techniques, in which we describe the high entropy alloy formed in arc suction melting furnace and its microstructural characterization were performed by using SEM and XRD. After performing the de-alloying process microstructural and mechanical characterization of the formed high entropy foams were carried out. Also surface modification techniques to enhance biocompatibility were discussed.

4.1 Alloy design

Mo, Nb, Ta, TI, Zr was selected as alloying elements due to their superior biocompatibility & non-cytotoxic behavior. The binary phase diagrams of selected elements were study. All the elements have negative enthalpy of mixing with each other which ensure the complete solubility of metals in molten form as well absolute homogeneity in solid state. To generate porosity, a filler element is required which demonstrate the complete solubility in molten state with all the selected metals and separation when solidified. After studying the binary phase diagrams of all the metals with number of elements from periodic table yttrium is selected as filler element because it has positive mixing of enthalpy with all selected metals which enable it to soluble completely with all the selected metals in molten form and completely insoluble in solidified form. Therefore, pseudo binary phase diagram of $(MoNbTaTiZr)_x$-$Y_{(1-x)}$ was calculated with Thermocalc software using the TCHEA database. Five different high entropy alloys were designed,

- S1-MoNbTaTiZr
- S2- $(MoNbTaTiZr)_{0.95}$-$Y_{0.05}$
- S3- $(MoNbTaTiZr)_{0.90}$-$Y_{0.1}$
- S4- $(MoNbTaTiZr)_{0.85}$-$Y_{0.15}$

- S5- $(MoNbTaTiZr)_{0.80}$-$Y_{0.20}$

And their respective foams are designated as FS2, FS3, FS4 & FS5 respectively. The designed compositions were superimposed on the pseudo binary phase diagram as shown in fig (4-1).

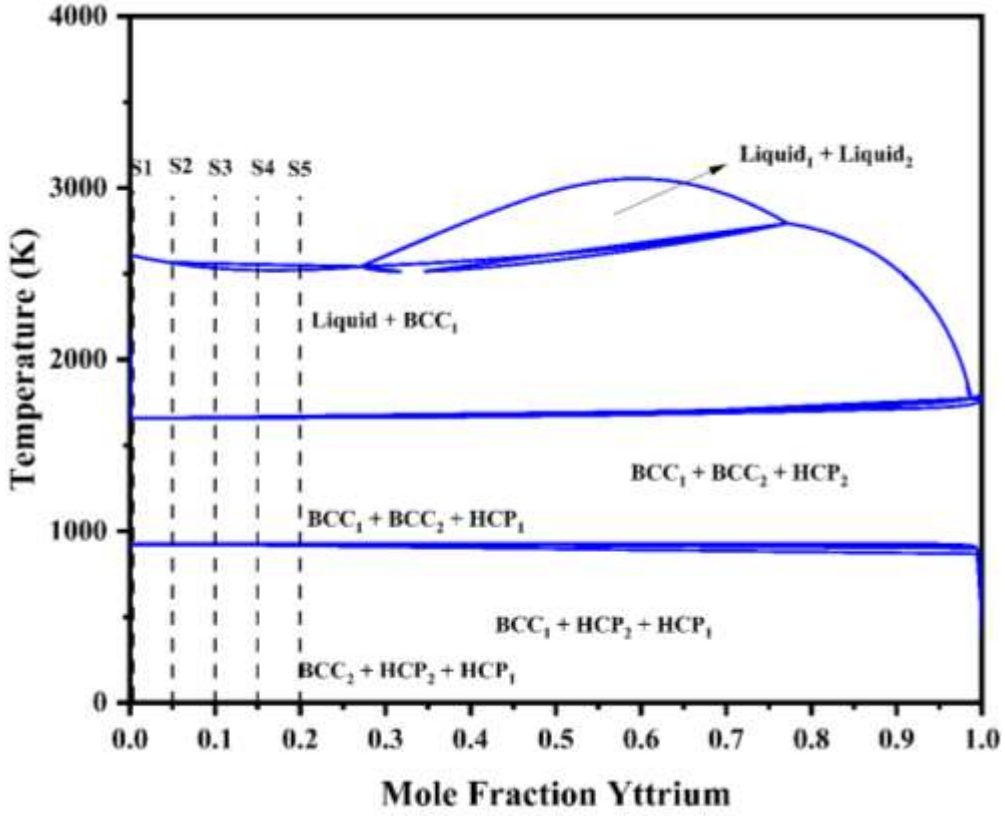

Figure 4-1 Pseudo binary phase diagram of temperature vs. mole fraction of Yttrium

Designed alloys have different compositions on the basis of varying concentration of filler element which intended to incorporate to form porous alloy after chemical dealloying process. Chemical etchant was carefully selected which reacts with filler element without reacting the other elements and successfully remove the yttrium. It was expected from phase diagrams of yttrium with all metal's yttrium shows complete separation in solidified state and move into inter-dendritic areas, therefore by removal of filler element by chemical dealloying process it is expected that 3d porous structure will form. To study the outcomes of our hypothesis, detailed microstructural study of dense and de-alloyed samples was carried out.

4.2 Characterization

4.2.1 Characterization of as-cast and developed high entropy foams

4.2.1.1 Crystal structure characterization

XRD results of as cast and porous samples are given in fig.4-2. Fig4-2(a) revealed that the as cast S1 HEA has dual-phase crystal structure, BCC1 (β1) and BCC2 (β2) phase, where BCC1 is major phase with high intensity prominent peaks whereas BCC2 is minor phase showing small peaks. Fig 4-2 (b, c, d, e) gives the comparison of crystal structure analysis for dense alloys with their respective porous high entropy foams. XRD analysis of high entropy alloys S2, S3, S4, S5 reveals the three-phase crystal structure identified as β1, β2, and Hcp (α-Yttrium) phase. However, the peaks intensity of α phase become significant as the yttrium concentration increases from S2 (5 wt.%) to S5 (20 wt.%). The XRD analysis of all de-alloyed samples reveals the presence of dual phase structure β1 and β2 and illustrates that the peaks of α phase diminish entirely by de alloying process.

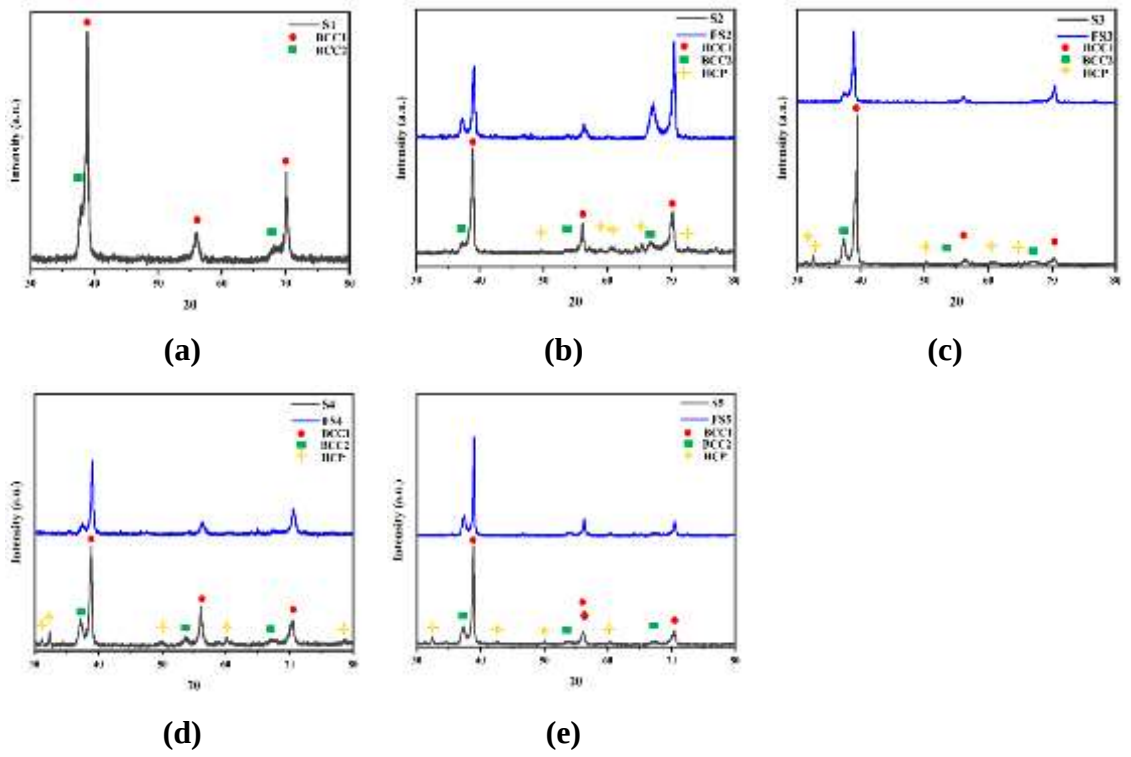

Figure 4-2 XRD patterns of (a) S1 (b) S2 & FS2 (c) S3 & FS3 (d) S4 & FS4 (e) S5 & FS5

4.2.1.2 Microstructure characterization

Microstructure analysis of as cast and de-alloyed samples are given in fig 4-3. Multiple contrasts are clearly visible in the microstructure of both as cast and porous samples. Only two regions (grey and light grey) are visible in the microstructure of as cast S1 HEA as shown in fig 4-3(i). EDS analysis in fig 4-3(a) revealed that light grey region is rich in Nb, Mo, Ta and represents the major BCC1 phase whereas grey region which is present in inter-dendritic region between the grain boundaries have high percentage of Ti, Zr and represents the minor BCC2 phase. Microstructure analysis of as cast HEA with zero concentration of filler element revealed that Mo, Nb, Ta forms the matrix while Ti and Zr move into inter dendritic region. The reason for this separation is miscibility gaps of Zr with Mo, Nb and specifically with Ta as present in the binary alloy diagrams, so two phases were form in the microstructure, Ta rich phase (Ta, Nb, Mo) and Zr rich phase (Zr, Ti). Titanium prefers to move with Zr due to miscibility gaps with Mo cause this dual phase partitioning effect. The melting point of Ta, Nb, Mo is higher than Zr and Ti, so after melting Ta, Nb, Mo solidifies early to form the BCC1 (β1) phase and formed the matrix, due to miscibility gaps push the Ti and Zr rich phase into inter-dendritic region and form the minor BCC phase (β2). The introduction of yttrium in the rest high entropy alloys produce significant changes in the microstructure. Microstructure characterization of all as cast high entropy alloys which incorporated some percentage of Yttrium shows three-phase microstructure characterize as light grey, grey and dark grey region. Ta rich phase (Mo, Nb, Ta) BCC1 solidifies first due to high melting points and miscibility gaps with Zr, Ti and yttrium to form the matrix by pushing the rest in inter-dendritic spaces. Zr rich phase (Zr, Ti) BCC2 solidifies along the grain boundaries of matrix due to huge miscibility gap with yttrium and restrict it into inter-dendritic region as clear in fig 4-4(a) and 4-4(b). It is confirmed from fig 4-4(a) and 4-4(b) that dark grey region presents in inter-dendritic region in fig 4-3(a, c, e, e) is yttrium. With the increase in yttrium concentration as we move from as-cast S2 to S5, inter-dendritic region increases.

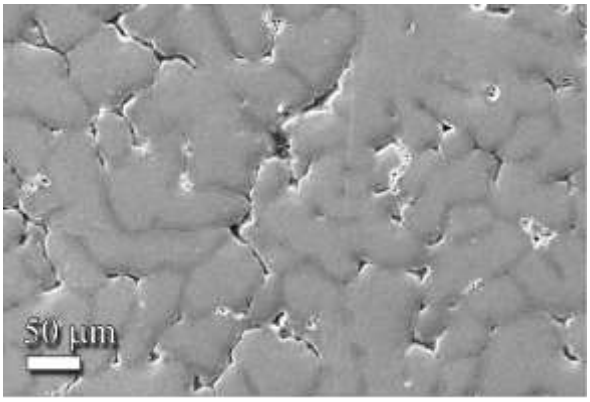

(a)

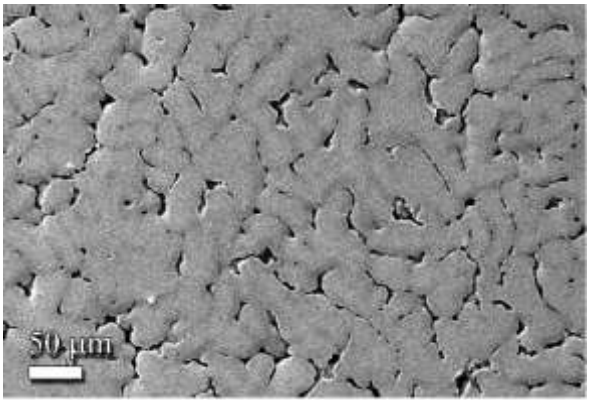

(b)

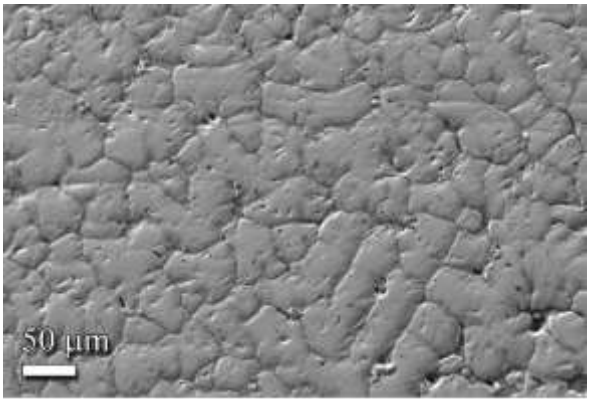

(c)

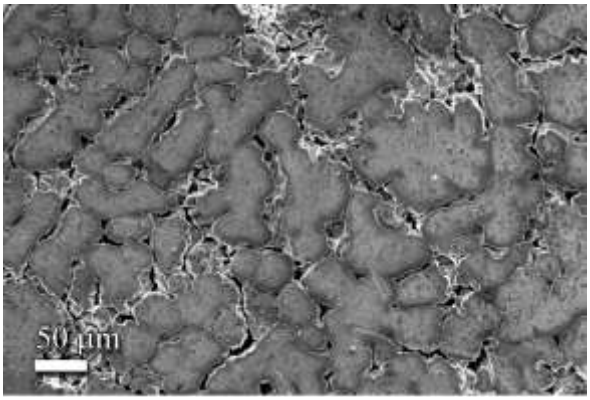

(d)

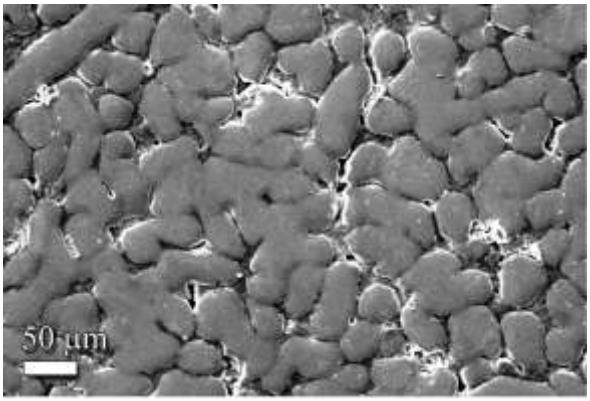

(e)

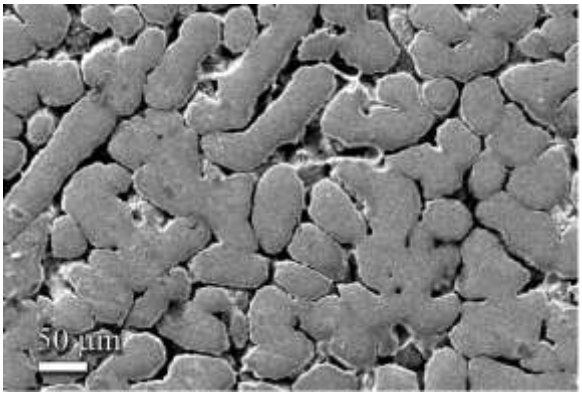

(f)

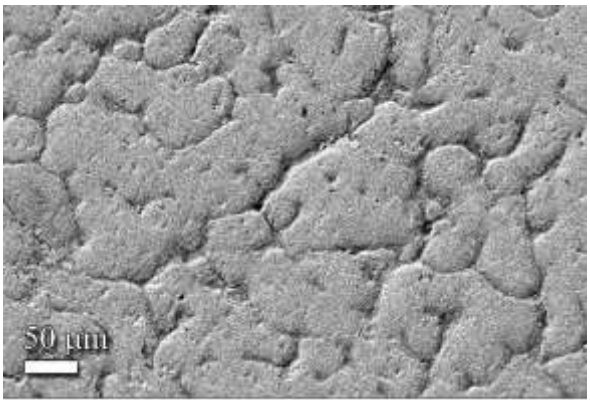

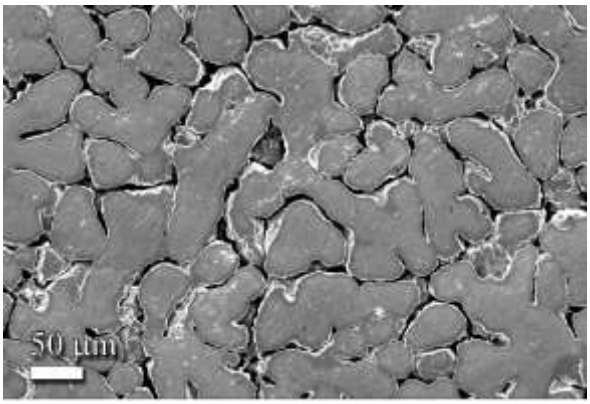

(g) **(h)**

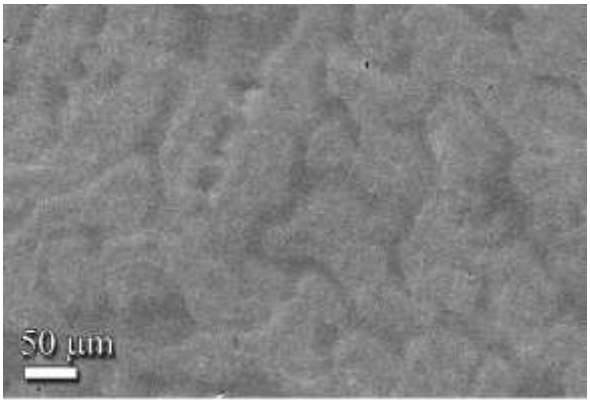

(i)

Figure 4-3 SEM analysis of (a) dense S2 (b) de-alloyed S2 (c) dense S3 (d) de-alloyed S3 (e) dense S4 (f) de-alloyed S4 (g) dense S5 (h) de-alloyed S5 (i) S1

On contrary in the microstructure of de-alloyed samples only two regions are visible, light grey and grey region as present in the case of S1 high entropy alloy which has no filler element present. As a result of dealloying process, yttrium is completely etched from inter-dendritic regions which results in the formation of 3d interconnected open pores. As clearly visible from the 4-3 (b, d, f, h) that the dark grey inter-dendritic region which were present in as-cast high entropy alloy completely diminished and connected channels are produced with BCC2 phase present along the grain boundaries and matrix consisting of Ta, Nb, Mo rich matrix BCC1 phase.

Fig4-4(a) and 4-4(b) shows the EDS analysis of sample S4 and FS4 respectively. The EDS results confirms the complete removal of yttrium HCP phase.

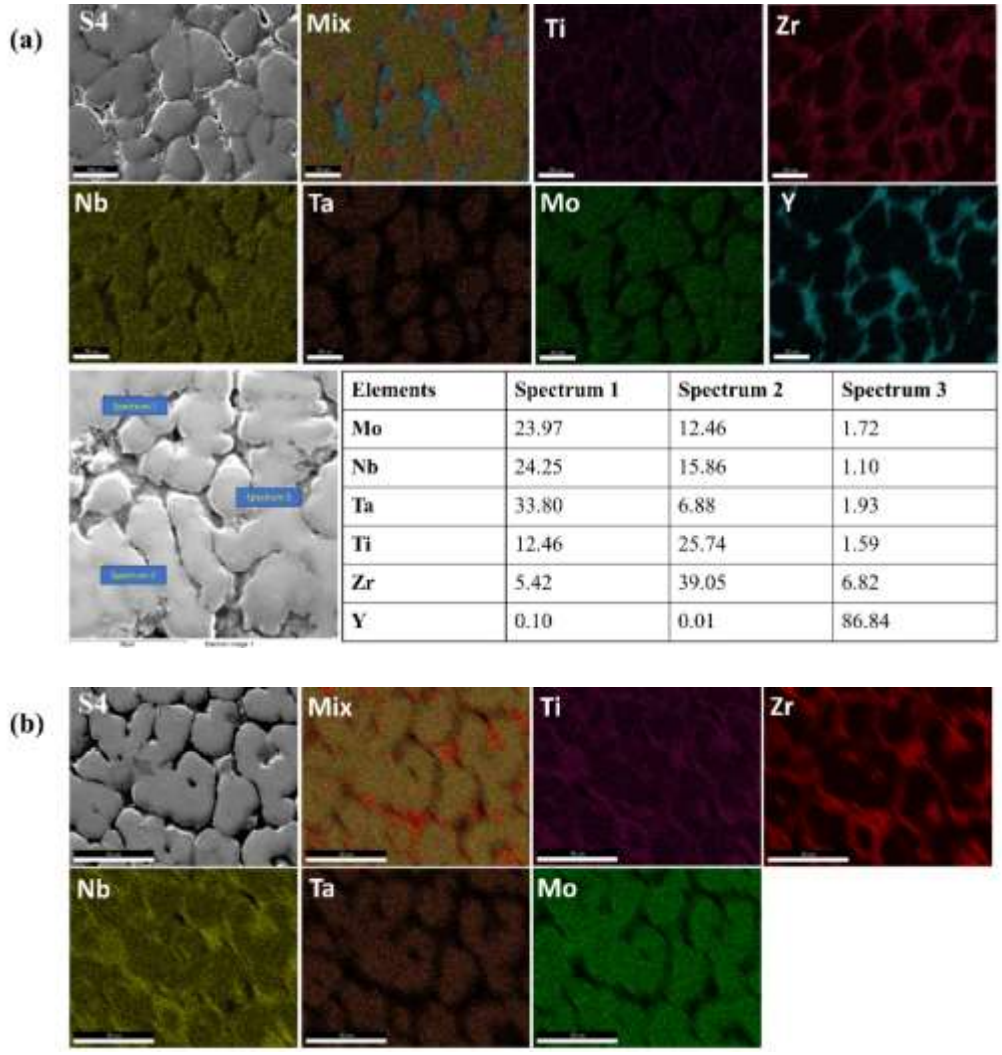

Elements	Spectrum 1	Spectrum 2	Spectrum 3
Mo	23.97	12.46	1.72
Nb	24.25	15.86	1.10
Ta	33.80	6.88	1.93
Ti	12.46	25.74	1.59
Zr	5.42	39.05	6.82
Y	0.10	0.01	86.84

Figure 4-4 EDS analysis of (MoNbTaTiZr)0.85-Y0.15 (a) S4 (b) De-alloyed S4

The SEM, EDS and XRD analysis results confirm the formation of high entropy foams, also these results are in accordance with the prediction of pseudo binary phase diagram.

The schematic of phase evolution during alloy solidification process is given in fig 4-5. At stage (a) the alloy is present in molten form. With decreasing in temperature, MoNbTa solidified to form alloy matrix having BCC1 phase and push the Zr, Ti and yttrium towards grain boundaries due to miscibility gap & lower melting temperature. At stage (c) Zr, Ti solidifies along with grain boundaries of matrix to form BCC2 phase and push yttrium

(HCP) in inter-dendritic spaces due to melting temperature difference and strong miscibility gap between Zr, Ti & yttrium. Chemical dealloying process occur in stage (e), during dealloying process yttrium is completely etched to form 3d porous microstructure as given in stage (f).

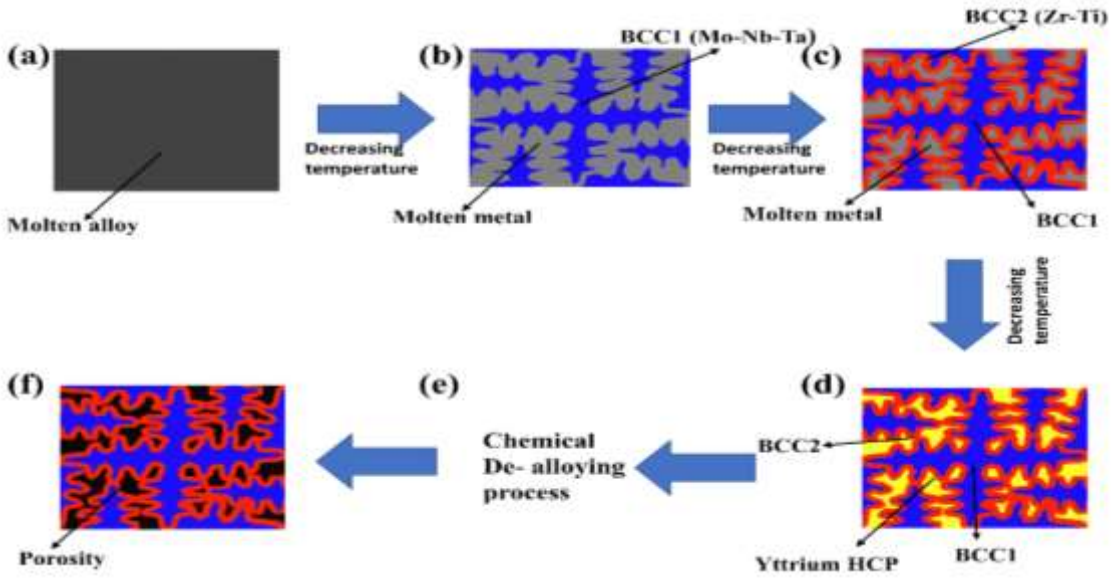

Figure 4-5 Schematic diagram of phase evolution during solidification and metallic foam formation

4.2.1.3 Gravimetric analysis

Gravimetric analyses were performed to confirm the removal of filler element and formation of high entropy foams. High entropy foams of as-cast alloys were formed with the introduction of porosity which was achieved by de-alloying process. Samples were dipped in the aqueous solution of nitric acid for 24 hours, the filler element added in the as-cast alloy were removed and high entropy foams were formed. The weight of alloys before and after dealloying process were measured and the weight loss due to the depletion of the filler element as function of filler element added given in fig 4-6.

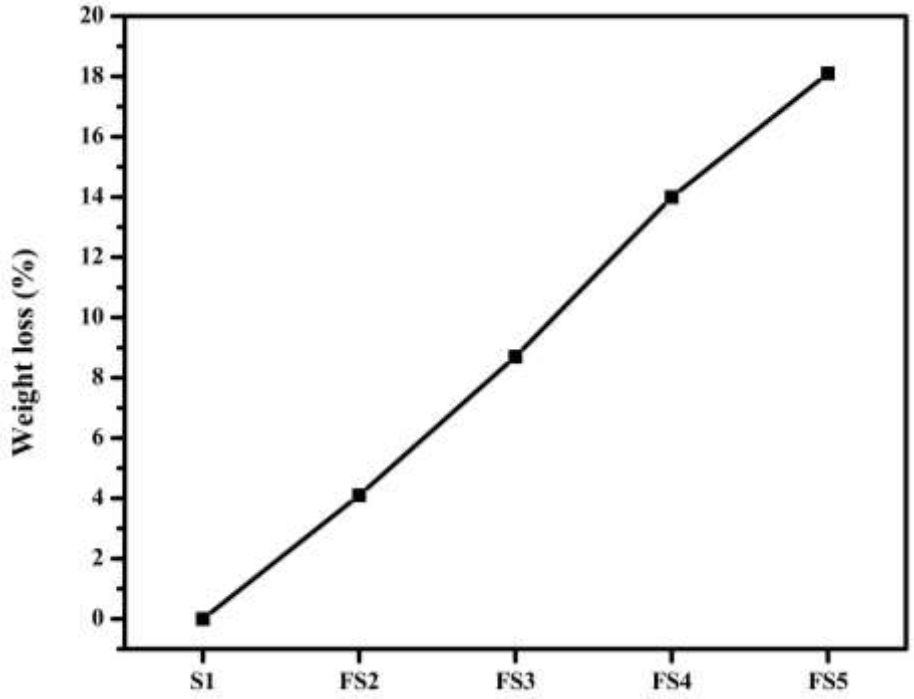

Figure 4-6 Weight loss in dealloying process

The percentage of weight loss increase accordingly with the amount of filler element incorporated in the as-cast alloys. Density was calculated with Archimedes' principle of dense(d_1) and de-alloyed samples(d_2), using the formula d_2-d_1/d_2 *100 gives the porosity percentage obtained. The value of porosity achieved are 4.1% for FS2, 8.7% for FS3, 14% for FS4 and 18.1% for FS5.

4.2.1.4 Mechanical characterization of high entropy foams

Mechanical properties of developed high entropy foams were evaluated with compression and Vickers hardness test. In Fig 4-7(a) compressive stress strain curves depicts a comparison between as cast and developed high entropy foams. The as cast HEA S1 demonstrate the highest value of elastic modulus 42.1 GPa whereas a decreasing pattern of elastic modulus observed with increasing porosity in developed foams. The high entropy foam FS5 revealed the lowest value of elastic modulus 3.6 GPa and maximum porosity (18.1%) in the understudy system. However, the decrease in elastic modulus drastically effects the yield strength and ultimate tensile strength which is undesirable. Yield strength and ultimate tensile strength of the high entropy foams was found to

decreases with increase in porosity from highest value 803 MPa and 1170MPa possessed by as-cast MoNbTaTiZr HEA to lowest value of 146.5 MPa and 231 MPa respectively, possess by S5 high entropy foam. Variation of elastic modulus, YS and UTS as function of porosity is given in fig 4-7(d,e,f). The results suggest that there is a large space available for adjusting the mechanical properties. The Vickers hardness with 100gf is given in fig 4-7(b). The values obtained for as-cast alloy is very high 507.2 HV than the bone 43.8HV. Hardness decreases exponentially with increase in porosity with minimum hardness obtained is 203.83HV for FS4, that is still considerably higher than the hardness of human cortical bone.

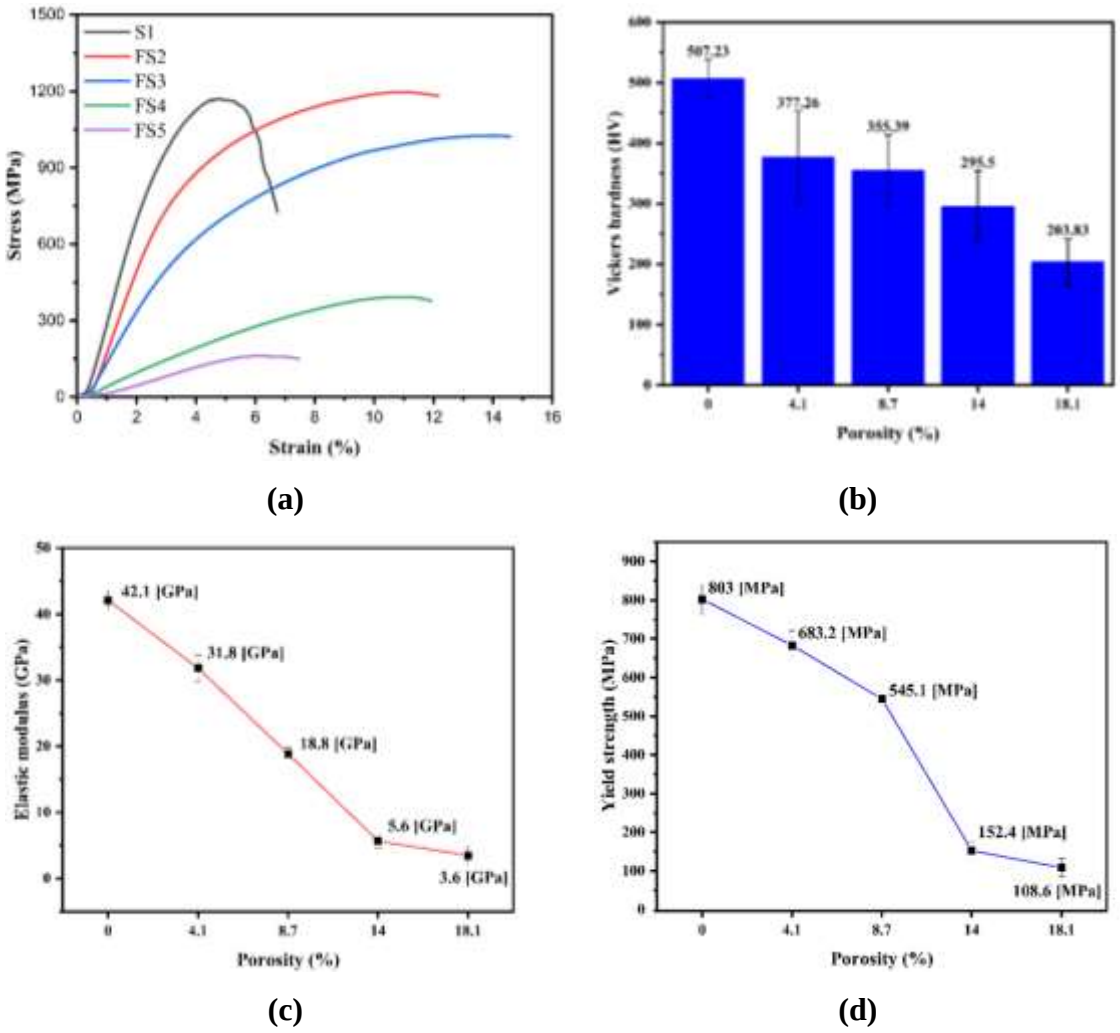

Figure 4-7(a) Compression testing graph of MoNbTaTiZr high entropy and foams (b) Vickers hardness testing graph of MoNbTaTiZr high entropy and foams (c) Elastic modulus vs porosity (d) Yield strength vs porosity

It is clearly evident from fig (4-7) that the as cast HEA MoNbTaTiZr and porous HE foams in this study possess ideal mechanical properties then the conventional implant materials employed.

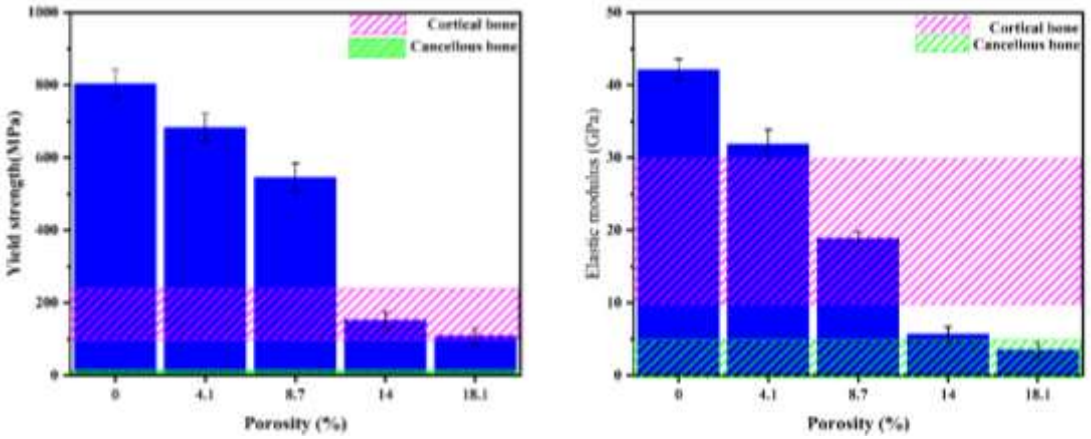

(a) **(b)**

Figure 4-8 Comparison of mechanical properties of High entropy foams with human bone (a) Elastic modulus (b) Yield strength

The elastic modulus of dense and porous alloys is given as function of porosity in fig 4-8a and compare the results with modulus of human bone. It is evident that dense alloy has high modulus then bone that can cause stress shielding effect leading to failure of implant. Whereas high entropy foams FS2 and FS3 shows comparable modulus with the modulus of cortical bone thus become promising candidate for the replacement of cortical bone. Moreover, FS4 and FS5 have similar modulus to cancellous bone therefore demonstrate potential alternative to cancellous bone.

Similar to elastic modulus the yield strength exhibit decreasing trend with increase in porosity. The developed foams FS2 and FS3 along with dense alloy revealed higher strength then the compressive strength of bone, hence showing strong potential for the replacement of cortical bone. However, FS4 and FS5 shows a rapid decrease in yield strength. The yield strength of FS4 and FS5 are comparable to cortical bone as clearly evident in fig 4-8b but due to cancellous bone's comparable elastic modulus, it is a favorable candidate for the replacement for cancellous bone.

The Ashby-type diagram mapping modulus versus strength in the perspective of biomaterials clearly demonstrates the unique features of formed high entropy alloy and foams in fig (4-9). The data from this study spans a large amount of "unoccupied space" at higher values of yield strength with lower elastic modulus when compared with the previously formed non-porous and porous metallic implants. This region can be considered as bridging the gap between the polymeric, metallic foams and metallic materials with superior mechanical strength at lower modulus. The formed high entropy foam's position on the Ashby diagram suggests that they could be employed as advanced materials for load bearing applications such as implants that require a mix of low stiffness and high yield strength.

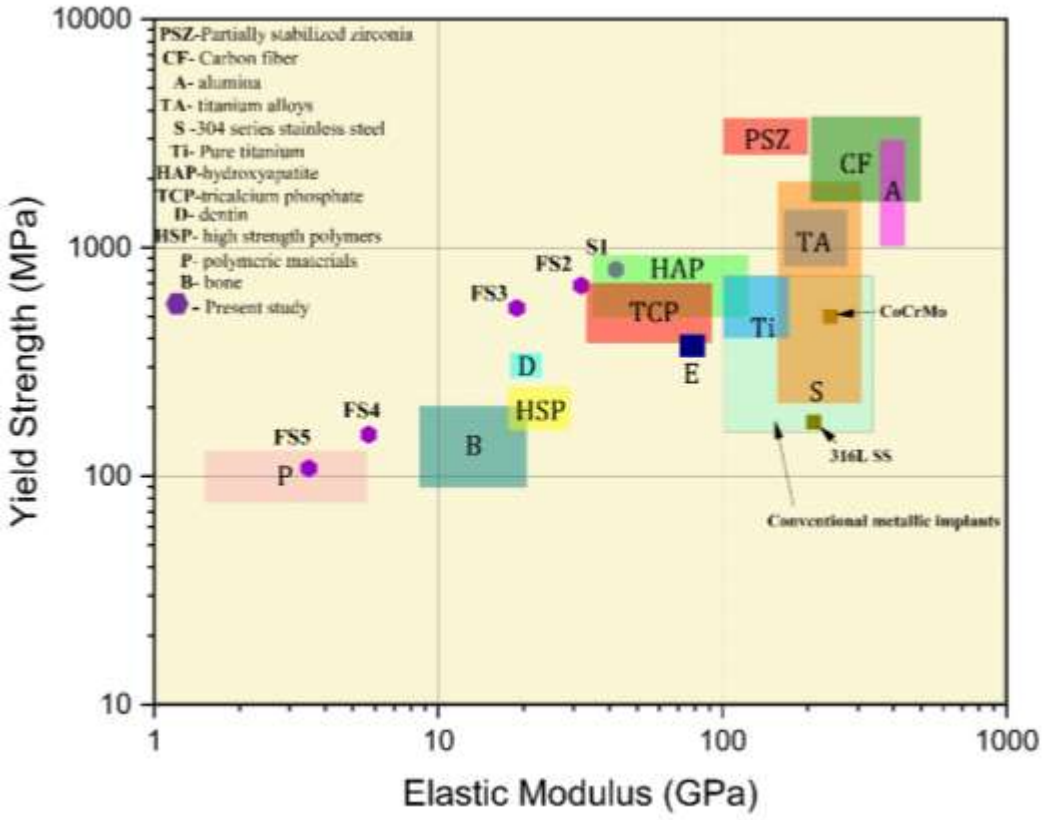

Figure 4-9 Ashby map diagram of Yield Strength vs Elastic Modulus

Elastic modulus of human bone lies in the range of (3-30) GPa, so the developed high entropy foams are particularly noteworthy as these have a range of comparable elastic modulus values (3.64-42) GPa with higher yield strength (108.5-803) MPa as compared

to bone. The elastic modulus of implants material should preferably match that of the bone to give a balanced load distribution between the prosthetic and the bone, because the health and healing of bone is intimately tied to the stress applied to it. The adjustable elastic modulus of the developed high entropy foams is of considerable value here as they may increase implant durability while lowering the risk of revision surgery. The yield strength values of the as-cast and developed foams are much higher than the UTS of human bones (50–195 MPa) demonstrating a considerable biomedical implant application potential.

4.2.1.5 Surface characterization of high entropy foams

Surface roughness of the developed high entropy foams were measured with atomic force microscopy analysis. AFM is a characteristics technique used to characterize the surface properties of the material. With the AFM analysis we measure the value of Ra, Rq and Rz. Ra is known as “Mean Roughness” and give us information about the about the height variations of material’s surface. Whereas Rq is known as “Root Mean Square Roughness” and gives information about the smoothness of the surface. Higher value of Rq means surface have higher roughness and vice versa. Rz is Known as “Mean Roughness Depth” and generally gives information about the highest peaks and deepest valley in the test specimen surface. The results of AFM analysis is shown in the form of graph below.

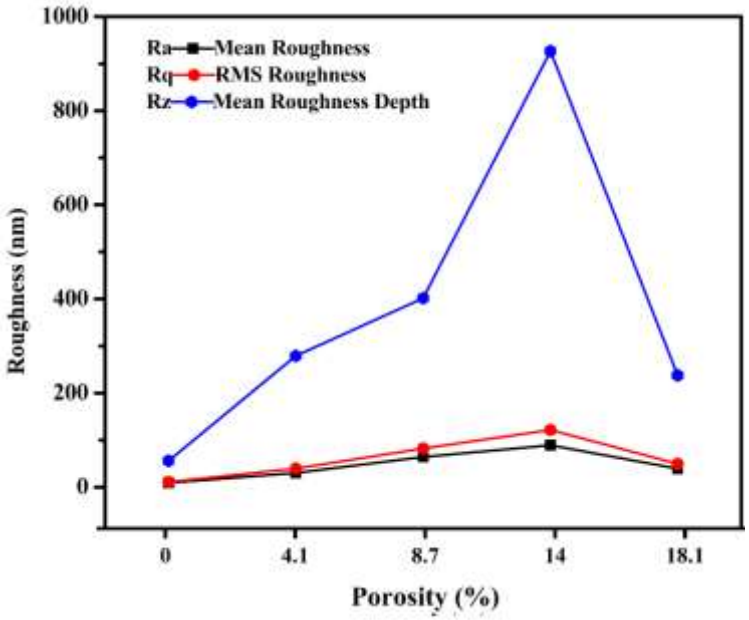

Figure 4-10 AFM results as function of porosity

The value of Ra and Rq increases proportionally with increases in porosity from S1 to FS4 and then decreases for FS5. That means the surface roughness has lowest value for MoNbTaTiZr having no porosity and increases directly as the percentage of porosity increases. The value of Rz also increases with the porosity because as the percentage of filler element present increases then dealloying process enhance its effect deeply in the alloy which results in larger difference between the highest point and deepest valleys present in the alloy surface. The Rz value is lowest for S1 having no porosity and increases with porosity till FS4 and then decreases for FS5. Higher surface roughness is desirable for biocompatibility of implants because high roughness make the surface hydrophilic and helps to promote osseointegration.

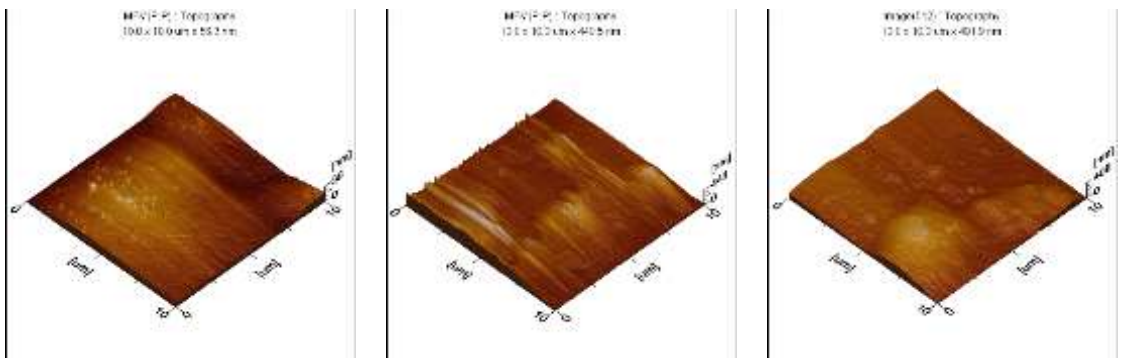

(a) **(b)** **(c)**

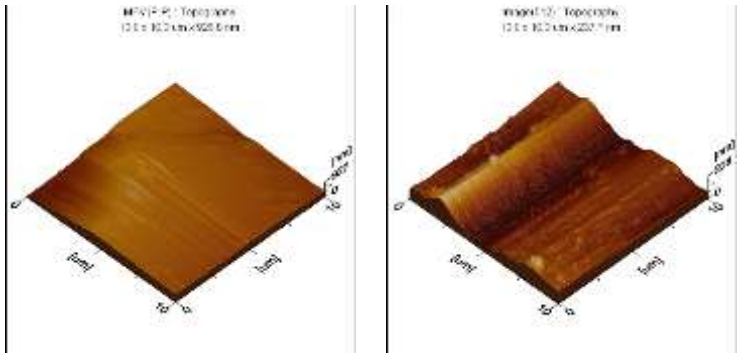

(d) **(e)**

Figure 4-11 3D micrographs of atomic force microscope for MoNbTaTiZr system (a) S1 (b) FS2 (c) FS3 (d) FS4 (e) FS5

4.2.1.6 Magnetic force microscopy of high entropy foams

Magnetic force microscopy of the developed foams was carried out to study the magnetic behavior of developed high entropy foams. MFM is magnetic characterization technique also present in the AFM machine. Titanium itself has a weakly magnetic moment and when a transition metal alloyed with it its magnetic properties increase. The musculoskeletal system is suited for MRI evaluation because of its good soft tissue contrast and its ability to give sectional representation of the human body in any plane and at any angle desired. But when a metallic implant is used in the body, patients' safety concerns raised which limits its full potential of MRI scanning. The loosening of implant and misplacement is an important issue with biomedical implants, but the use of metallic implant which have strong magnetic susceptibility limits the MRI use for imaging and need for new imaging methods arising. Also, if the magnetic susceptibility of the implant used is high then loosening and misplacement of implants take place and caused serious concerns which is harmful for the body. So, when a metallic implant used, it should have least magnetic susceptibility.

The magnetic force microscopy results of the developed alloys are given below

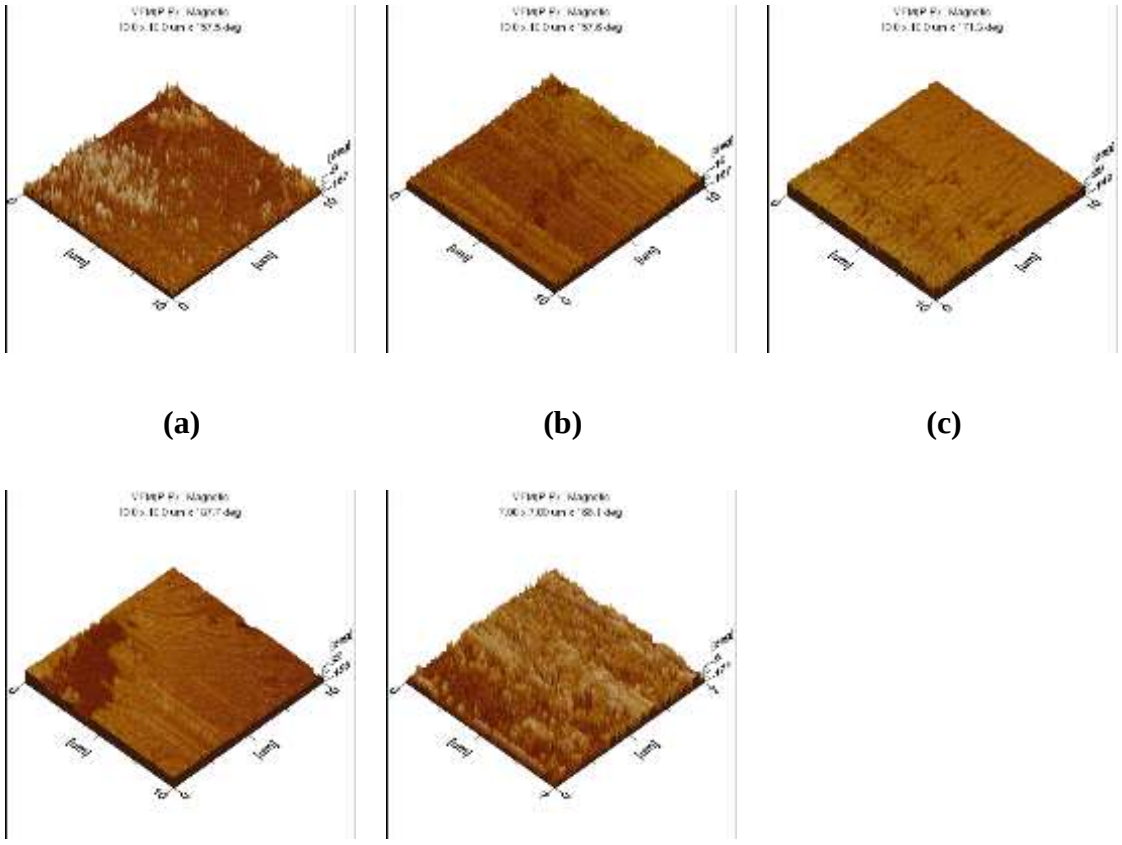

(a) **(b)** **(c)**

(d) **(e)**

Figure 4-12 3D micrographs of magnetic force microscope for MoNbTaTiZr system (a) S1 (b) FS2 (c) FS3 (d) FS4 (e) FS5

The light brown areas shown in the figures above represent the presence of magnetic material. The as-cast high entropy alloy S1 having no porosity in its microstructure shown weak magnetic susceptibility whereas no indication of light brown regions appeared in the developed high entropy foams except FS5 having maximum porosity shows large amount of light brown area which means S1 and FS5 have higher magnetic susceptibility while other three developed foams having FS2, FS3 and FS4 are very weak or negligible magnetic susceptibility which is requirement of biomedical implant and cause no limitation during MRI imaging. However, magnetic properties are not entirely harmful for the body. Weak magnetic properties are beneficial in the development of bone and tissue repairing. It helps in the alignment of macromolecules and osteoblast in the body. Because of the magnetic action, molecules aligned in the porous channels, resulting in quicker cell

transport to the bone and tissues. The faster transport of vital cells to the bone and tissues also depends on the amount and interconnectivity of porous channels. So, higher the percentage of porosity results in quicker transport of cells to bone and tissues which stimulates the anchoring of implant with the adjacent bone and healing the damage tissues.

4.2.1.7 Contact angle analysis

For better osseointegration and cell proliferation hydrophilic surface of the implant material is desirable. Contact angle analysis of the developed foams were carried out and compared the results with the as-cast alloy S1 which have no porosity present to study the hydrophilic behavior. Hydrophilicity is defined as the surface is hydrophilic when the contact angle of the water droplet with the surface is less than 90 degrees. The results of contact angle analysis are given in figures below.

(a)

(b)

(c)

(d)

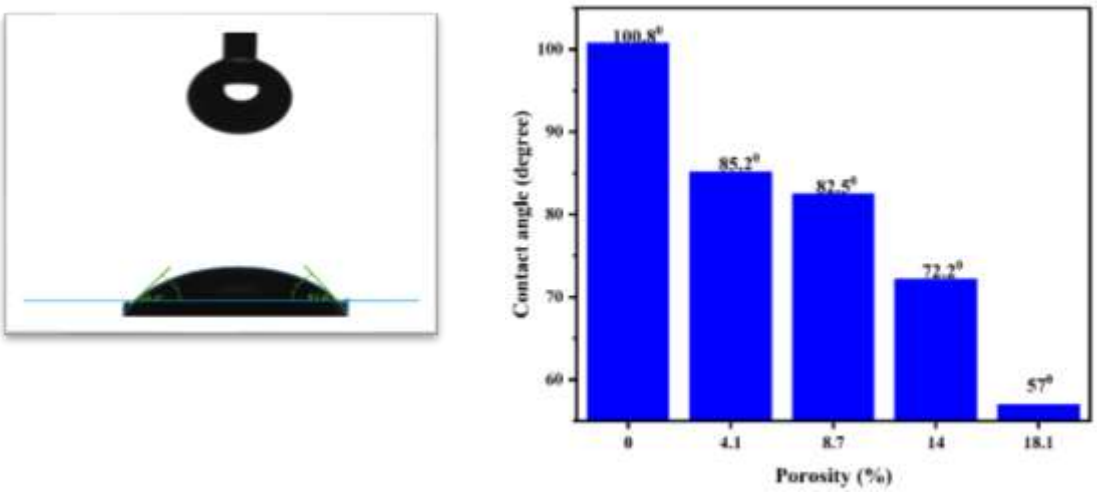

(e) **(f)**

Figure 4-13 Contact angle analysis of MoNbTaTiZr system (a) S1 (b) FS2 (c) FS3 (d) FS4 (e) FS5 (f) Contact angle vs porosity

The contact angle of the as-cast alloy is greater than 90 degrees categorize as hydrophobic in nature which is not desirable for bio-implant applications. As the percentage of porosity increases in the developed alloys the value of contact angle decreases from 88 degrees for (FS2) to 57 degrees for (FS5). These results indicate that with increasing porosity, hydrophilicity of the implant surface enhanced which means that biocompatibility increase with increase in porosity.

4.2.1.8 Brunauer–Emmett–Teller (BET) analysis

BET analysis was used to determine the specific surface area of the developed high entropy foams. The total volume of pores and average pore size formed as a result of the dealloying process are also determined by BET analysis. BET results revealed that with increasing the percentage of porosity surface area increase proportionally of the formed high entropy foams. Large surface area per unit of bulk metal surface is desirable for success of bio-implant because it offers large area to bone for load transfer against the implant surface. Therefore, with the introduction of porosity and in result increase of surface roughness offer large surface area for bone attachment. The graphical representation of the BET results about surface area are shown in figure 4-14(a). Total

volume of pores also calculated with the BET analysis. The results indicate that with the increase in the porosity percentage, total volume of pores also increases proportionally. The graphical representation is given in fig 4-14(b).

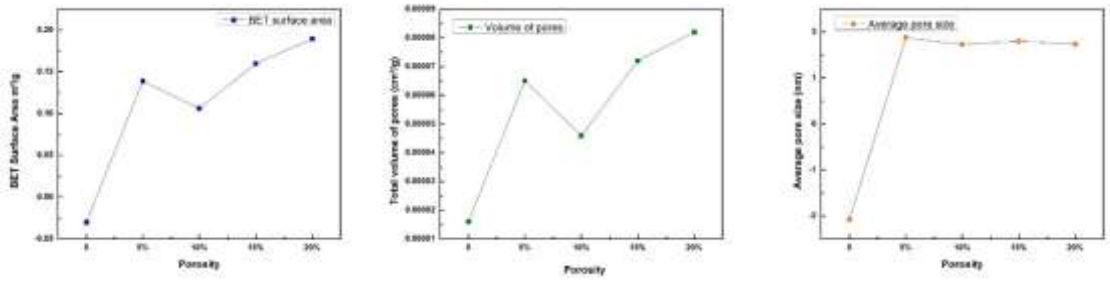

(a) **(b)** **(c)**

Figure 4-14 Brunauer–Emmett–Teller analysis of MoNbTaTiZr system (a) Surface area vs porosity (b) pores volume vs porosity (c) Average pore size vs porosity

BET analysis revealed that the porosity in the developed high entropy foams is micro and meso porosity. Micro and meso-porosity are desirable for cell attachment and transfer of essential enzymes from the body fluid to bone and tissues. The porosity present in the understudy system is interconnected to form long porous channels which have length from 1μm to about 30μm approximately. So, we can conclude that formed high entropy foams have micro, meso and macro porosity (interconnected porous channels) is present which is essential and desirable for cell attachment, transfer of cells and enzymes to the bone and attached tissues results in faster growth of bone and healing of damage tissues.

4.2.2 Surface modification of the high entropy foams

4.2.2.1 Surface modification of the high entropy foams by hydroxyapatite coating

Bio-mimetic coating of hydroxy apatite on developed foams were carried out by immersing the samples in simulated body fluid for 10 days at 37^{o}C. Hydroxyapatite coating enhanced the osseointegration of the implant in the body and helps in good fixation of implant with the adjacent bone and tissues. Gravimetric analyses were carried to ensure the deposition of hydroxyapatite on the samples surface. The weight of the samples was

measured before immersing the samples in the SBF and again after 10 days when samples retrieved from the solution. The weight percentage results are given in the graphical form below

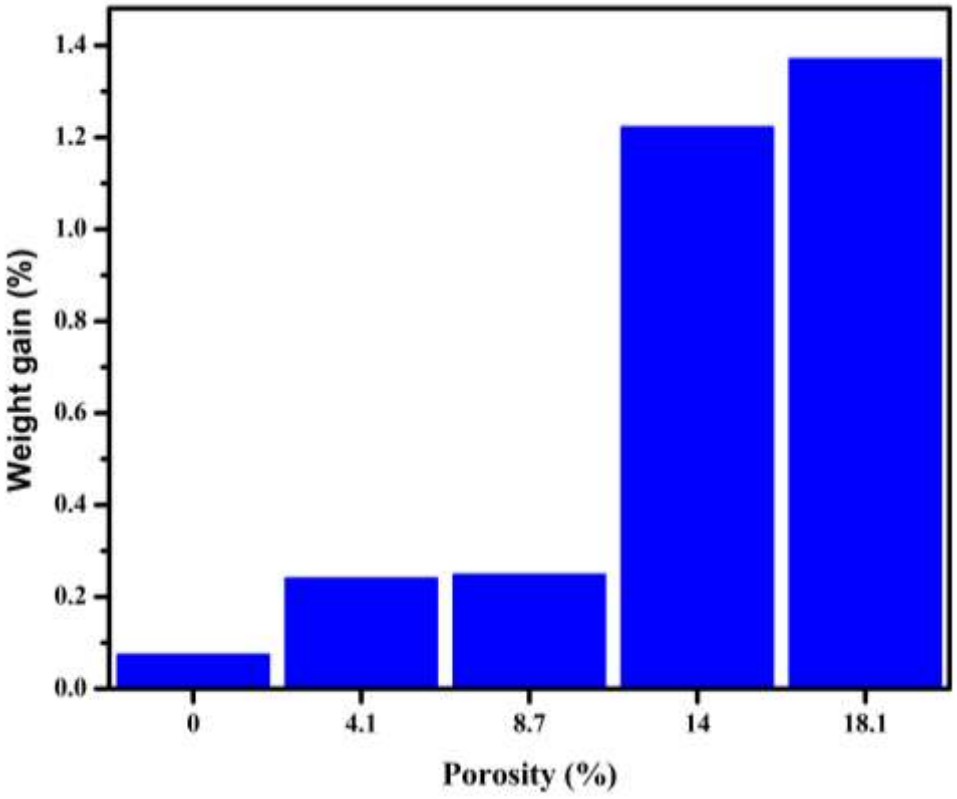

Figure 4-15 Weight gain vs Porosity in Simulated body fluid

The gravimetric analyses shows that the samples which had high porosity gain more weight than other counterparts. The as-cast alloy S1 which have no porosity show very small weight gain while FS5 has maximum percentage of porosity present in its microstructure and shows maximum weight gain. The results indicated as we can analyze the graphical representation weight gain increase proportionally with the porosity in the foams. This occurs because increase in porosity results in increase of specific surface area as BET results demonstrated which provide more available area for HA coating. Also, AFM and contact angle results indicated that with the increase porosity the surface roughness increases, and contact angle decreases which is favorable for HA coating. During this process prepared samples of the developed were immersed in the solution,

whereas the solution changes after every two days with the fresh solution to maintain the pH and ion concentration of the solution.

4.2.2.1.1 Microstructural characterization of HA coated samples

Microstructural analysis of HA coated high entropy alloy/foams were carried out with scanning electron microscope.

In the microstructure of S1 as-cast high entropy alloy there are little HA deposition seems on the surface. We can explain this as, absence of porosity leads to lower surface roughness and hydrophilicity, which became reason of little deposition even after a 10-day immersion in SBF. EDS analysis confirm presence of calcium and phosphate on the surface in very small percentage. In the SEM image of FS2 high entropy foam HA deposition is clearly visible. HA grows on the grain boundaries and in the porous channels present on the surface of foam. Fig 4-16(c, d, e) demonstrate that the HA deposition enhanced proportionally with the increase in porosity. The SEM image of FS2 revealed that the whole surface is covered with hydroxyapatite coating. We can conclude here that as the amount of porosity increases more pores and porous channels available for the growth of HA. Also as discussed above with the increase in porosity, surface roughness enhanced significantly, contact angle decreases and specific surface area increases which results in HA deposition in large amount.

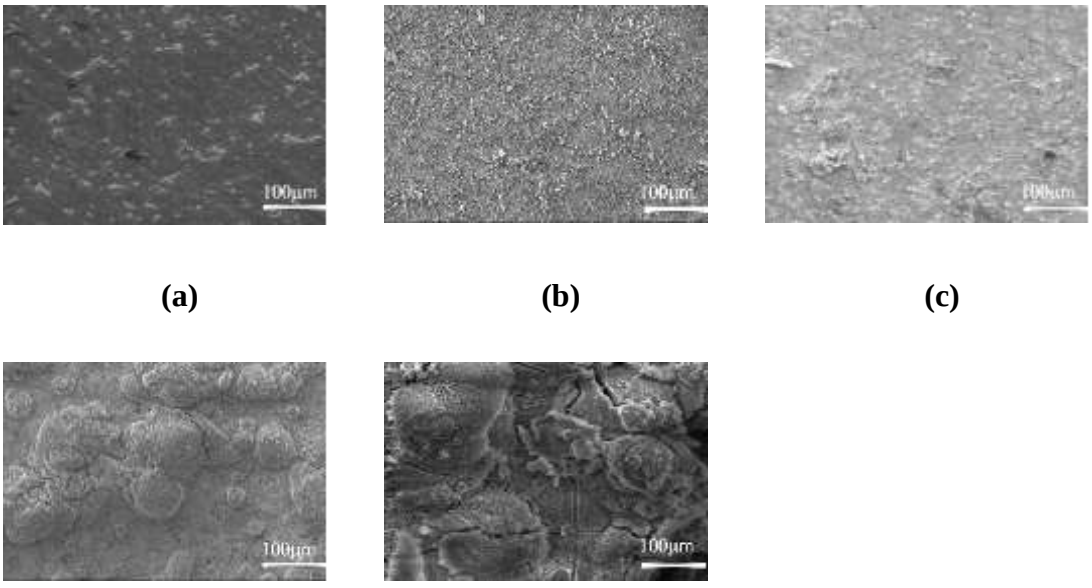

(a) **(b)** **(c)**

(d) **(e)**

Figure 4-16 SEM results for hydroxyapatite coated samples (a) S1 (b) FS2 (c) FS3 (d) FS4 (e) FS5

4.2.2.1.2 Contact angle analysis of HA coated samples

The developed foams and as-cast samples are coated with hydroxyapatite. When implant is placed in the required place in the body, its surface interacts with the adjacent bone, tissues, and body fluid. To minimize its settlement duration in the body, avoid the foreign body response and provide strong attachment with the bone, HA coating of the implant surface is carried out. HA coating on the implant surface mimic the bone and slow down the chemical reactions occur immediately on the metal surface after placement of implant in the body. HA coating also increase the rate of bone growth because it increases the hydrophilicity. Contact angle results of the HA coated samples are given below. In the surface of as-cast alloy, little amount of HA coating appears as compared to the porous samples and due to this moderate HA deposition, its contact angle decreases to 78 which make its surface hydrophilic. From the contact angle results of other high entropy foams, we concluded that the contact angle decreases proportionally with the increases in porosity percentage. Contact angle results also be defined in the term of HA deposition on implant surface, the contact angle decreases as the HA deposition on implant surface increases.

(a) **(b)**

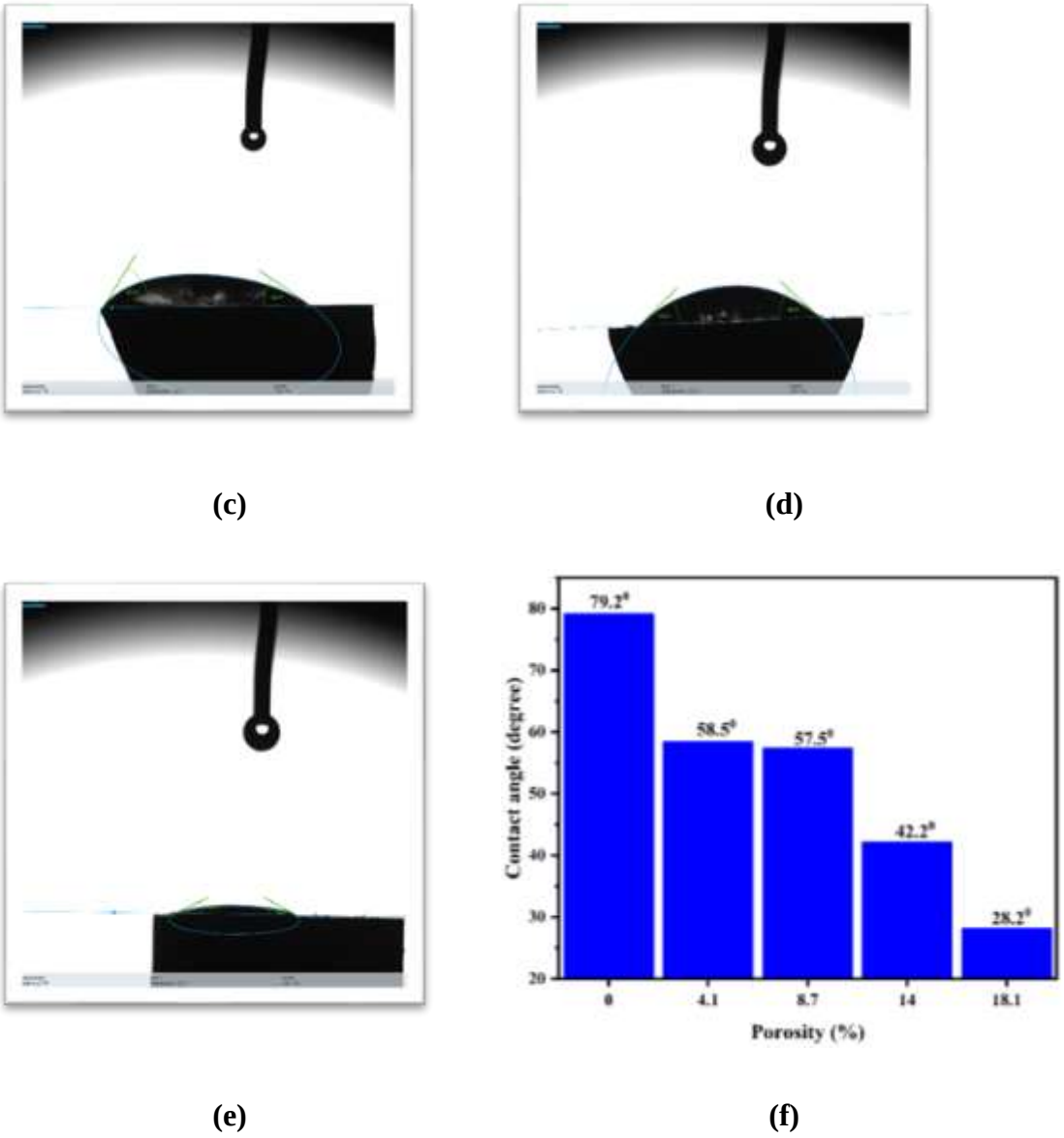

Figure 4-17 Contact angle analysis for hydroxyapatite coated samples (a) S1 (b) FS2 (c) FS3 (d) FS4 (e) FS5 (f) Contact angle vs porosity

4.2.2.2 Alkali treatment of developed foams

When metallic implant is introduced in the body, number of biological and chemical reactions occur on its surface, so excellent chemical stability of implant surface is required to avoid the release of toxic elements in the body. Also, after the placement of implant in the body new bone growth in the surrounding of implant and the deposition of bone on the implant surface takes place through osteo-conduction. However, in the case of metallic

implant, the implant surface and bone osseointegration process is limited due to its low affinity with the living bone. This causes the foreign body response. Moreover, when metallic implant placed in the body, the implant surface is isolated from the living bone by fibrous tissues which reduce the healing rate. In some cases, rapid healing is essential for the successful osseointegration but due to very slow bone formation on the implant surface as we discussed above results in failure of implant.

Alkali treatment of implant is a surface modification technique which is employed to enhance the bioactivity and make its surface attractive for quick bone formation. When the HA coated metallic implant is placed in the body then due to the brittleness and weak bonding between the HA layer with implant surface, coating is detached from the implant and results in the inhomogeneous composition distribution of blood. Therefore, alkali treatment is chemically surface modification treatment increase the bioactivity and promote the osseointegration. The hydrophilicity of the alkali treated implant surface is significantly enhanced and the uniform and quick HA deposition takes placed results in rapid healing.

For alkali treatment, the samples were soaked in 5M NaOH solution at 60^0C for 24 hours. Gravimetric analysis is used to compare the HA deposition with and without alkali treatment. So, weight of samples was measure before and after the alkali treatment. After alkali treatment samples were immersed in simulated body fluid and measure the weight again. SEM of the alkali treated and HA coated samples after alkali treated were carried out and compare them with the results obtain with only HA coated foams without alkali treatment. The results revealed that the alkali treated HA coated samples have higher amount of HA deposition with uniform coating all over the implant surface compared to the only HA coated samples which have clots of HA deposition in mainly on the grain boundaries and in the porous channels.

The gravimetric analysis of alkali treated and after immersion in SBF are shown in graphical form below.

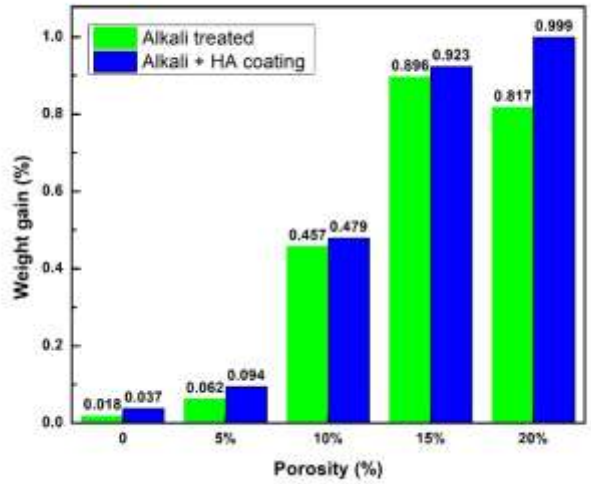

Figure 4-18 Weight gain vs porosity of alkali treated samples after hydroxyapatite coating

The results demonstrate that the as-cast sample having no porosity shows less weight again even after the surface activation with alkali treatment. All the other samples revealed that the samples gain weight after alkali treatment with the increase in the porosity. The highest amount of weight is gained by sample FS4 while the lowest amount of weight gained by S1. Unexpectedly FS5 gained less weight than FS4, which may be due to some fault in sample preparation or sample handling or may be due to the placement of sample in wrong direction during the alkali treatment. However, after the alkali treated samples immersed in simulated body fluid, the lower amount of weight is gained by the S1 dense sample and highest weight gained by the FS5. Herein, we can conclude that the HA deposition is proportional to increase in porosity.

4.2.2.2.1 Microstructural characterization of alkali treated high entropy foams

SEM analysis of high entropy foams/alloy were carried out after alkali treatment for microstructural characterization. After alkali treatment samples were washed with deionized water and dried in air for further characterization and treatment.

The SEM image alkali treated S1 high entropy alloy show no significant deposition of sodium titanate layer on the alloy surface which is due to low surface roughness and large contact angle (hydrophobic nature). The alloy surface is clearly visible and small particles

deposited appeared only in a fewer spot. In the SEM image of FS2 the growth of sodium titanate layer observed on the grain boundaries and in the porous sites. With the increase in porosity the sodium titanate layer grows significantly in the porous channels present on the FS3 high entropy foam surface and cover the surrounding areas. In the SEM image of FS4 high entropy foam it is evident that the whole surface is covered with a sodium titanate layer, with not a small portion of foam surface visible. The sample surface of FS5 is completely covered with the sodium titanate layer. It can be seen in the SEM image that the sodium titanate grows in the porous channels and due to high percentage of porosity in the alloy surface porous channels are interconnected and the sodium titanate layer which grows in the porous channels also covered the adjacent area of the grain results in the whole coverage of the foam surface. The increase in porosity surface roughness increases accordingly, the specific surface area increases provide more nucleation sites and contact angle decreases which made the surface hydrophilic. All these functions are responsible for higher growth of sodium titanate layer and become favorable with the increase in porosity.

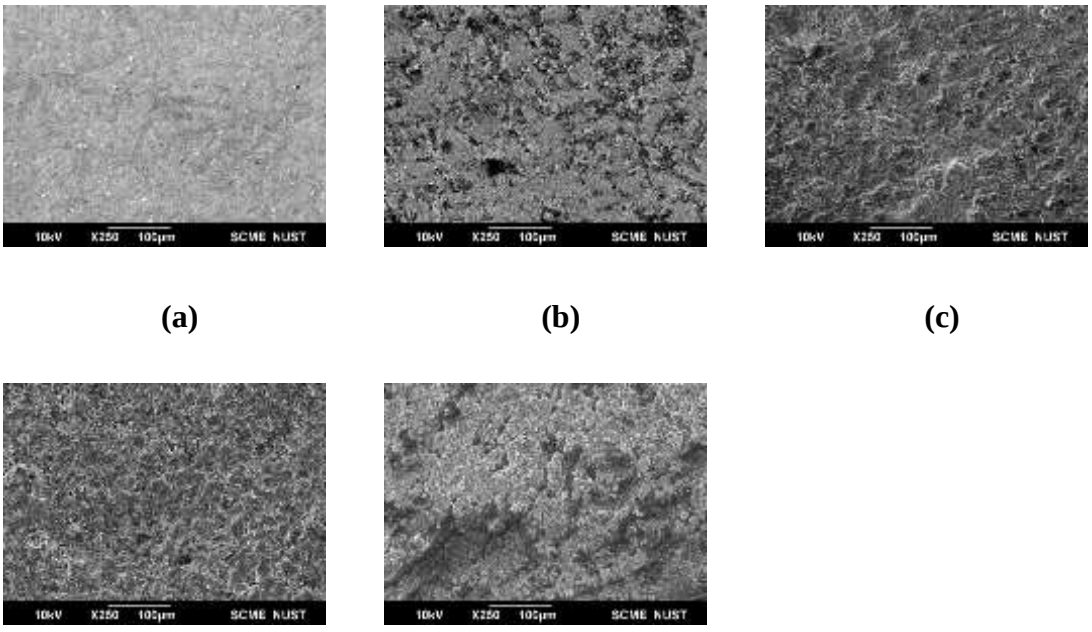

(a) **(b)** **(c)**

(d) **(e)**

Figure 4-19 SEM results for alkali treated samples (a) S1 (b) FS2 (c) FS3 (d) FS4 (e) FS5

4.2.2.2.2 Contact angle analysis of alkali treated samples

Contact angle analysis of the alkali treated samples were carried out to study the effect of alkali treatment on hydrophilicity of the sample. It is observed that the contact angle of alkali treated samples decreases significantly as compared to the untreated samples. Also, the results revealed that the contact angle decreases proportionally as the growth of sodium titanate layer increases on samples surface which is defined as with the increases in porosity on test samples sodium titanate layer growth increases directly as demonstrated by the SEM and gravimetric analysis.

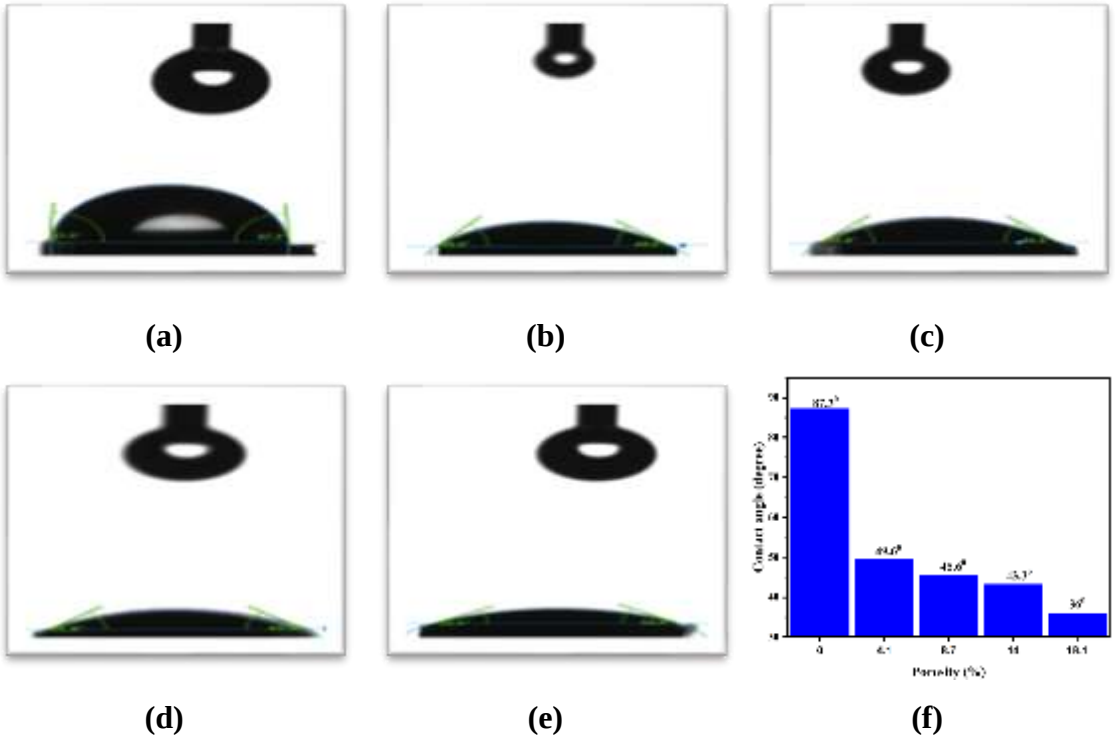

Figure 4-20 Contact angle analysis for alkali treated samples (a) S1 (b) FS2 (c) FS3 (d) FS4 (e) FS5 (f) contact angle vs porosity

4.2.2.3 Bio-mimetic coating on alkali treated samples

Alkali treated samples were immersed in simulated body fluid for HA coating. This process is also used to study the bone forming ability after placement in the body. Due to the surface activation through alkali treatment and increase in hydrophilicity, so it was supposed that the uniform and early HA coating formed on the sample surface then the

untreated samples. The SEM, contact angle and gravimetric analysis results were compared with the HA coated samples without alkali treatment.

4.2.2.3.1 SEM analysis of alkali treated hydroxyapatite coated samples

As discussed in the above paragraph the surface is activated and hydrophilicity enhanced significantly by alkali treatment, it is expected that the HA deposition occur early and homogeneous throughout the surface of test sample because in the case of untreated samples porosity present on the surface act as active sites for deposition but in the case of alkali treated samples all the surface is chemically activated which results in uniform HA deposition.

In the SEM image of S1 as cast alloy, it is visible that HA deposition takes place but in small amount and coating is spread over the sample surface in form of small regions. From the SEM image and gravimetric analysis, we can say that alkali treated sample have some traces of HA deposition as compared to untreated HA coating sample of S1. In the SEM image of FS2, it is visible that the HA deposition takes place and distributes uniformly on the surface as compared to the untreated sample of FS2 on which HA nucleation takes place only at the sites where porosity and porous channels are present. With the increase in porosity the high entropy foam FS3 show high amount of HA deposition and the HA coating disperse on the surface instead to form HA clusters on the porous sites. In the SEM image of FS4 the whole surface of the alkali treated foam is covered with HA coating and the main difference from untreated HA coated samples are the surface is homogeneously covered with HA coating and no clusters formed on the surface which is clearly visible from the SEM image. The SEM image of FS5 demonstrate that the whole surface of the alloy is covered with HA coating. A thick layer of HA coating formed, and no region of substrate surface is visible.

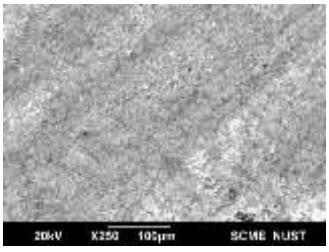

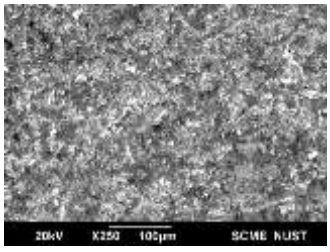

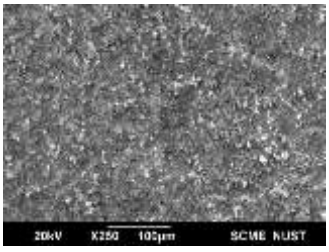

(a) **(b)** **(c)**

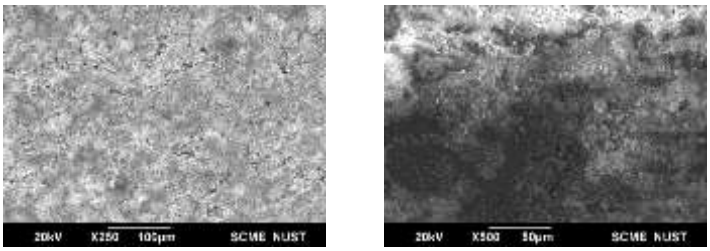

(d) **(e)**

Figure 4-21 SEM results for alkali treated hydroxyapatite coated samples (a) S1 (b) FS2 (c) FS3 (d) FS4 (e) FS5

4.2.2.3.2 Contact angle analysis of alkali treated HA coated samples

The contact angle analysis of alkali treated HA coated samples were carried out to study the effect of uniform HA coating after alkali treatment on the hydrophilic behavior. The contact angle analysis results are shown in figure below. From the contact angle results we conclude that the contact angle decreases with the increase in HA coating deposition on the surface which is directly related with the increase in porosity. Therefore, we can say that with the increase in porosity surface roughness, specific surface area increases, and hydrophilicity enhanced., in result during alkali treatment the growth of sodium titanate layer enhanced. More HA deposition takes place on the alkali treated samples having higher growth of sodium titanate, so if conclude all these parameters we can say that the hydrophilicity enhanced significantly with the increase in porosity.

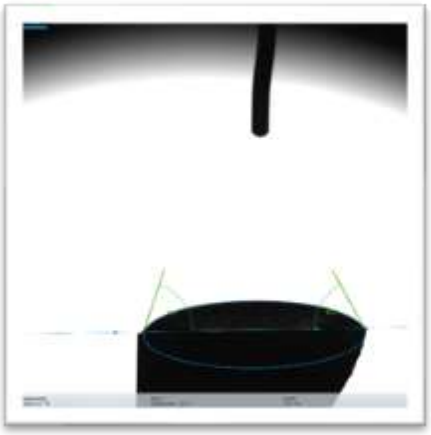

(a)

(b)

(c)

(d)

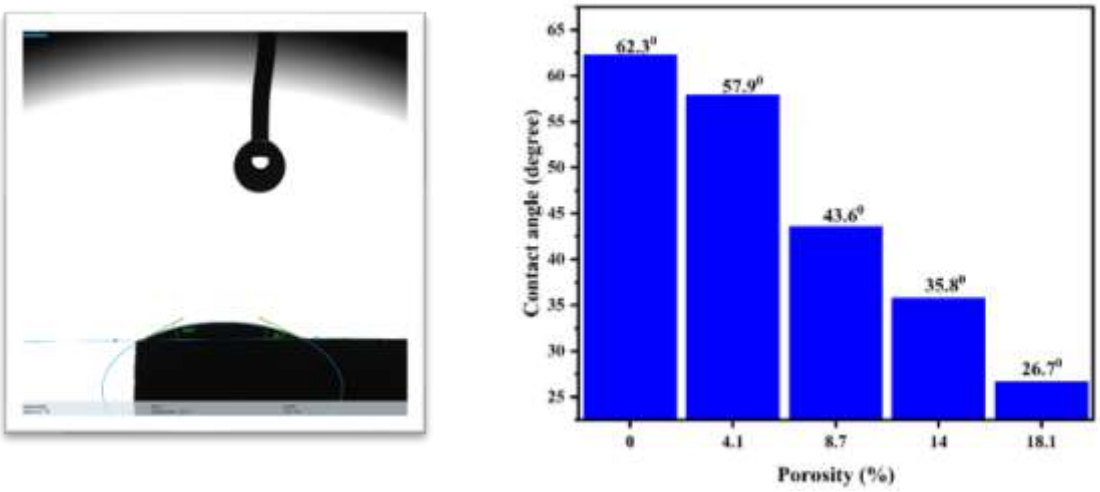

(e) **(f)**

Figure 4-22 Contact angle results for alkali treated hydroxyapatite coated samples (a) S1 (b) FS2 (c) FS3 (d) FS4 (e) FS5 (f) Contact angle vs porosity

4.2.2.3.3 Fourier transform infrared spectroscopy

The FTIR results of alkali treated HA coated samples in graphical form given in fig 4-22. The FTIR spectrum shows the presence of carbonate and phosphate bands. The absorption bands of O-H group are detected at around 3600 cm−1, 1600 cm−1 and 600 cm−1, whereas the characteristic peaks of carbonate groups are detected at around 1500 cm−1 and 800 cm−1. The absorption bands of phosphate bands are observed at around 1000 cm−1 and 600 cm−1. The FTIR results confirm the presence of carbonate and phosphate precipitation on the HA coated samples (through bio-mimetic coating).

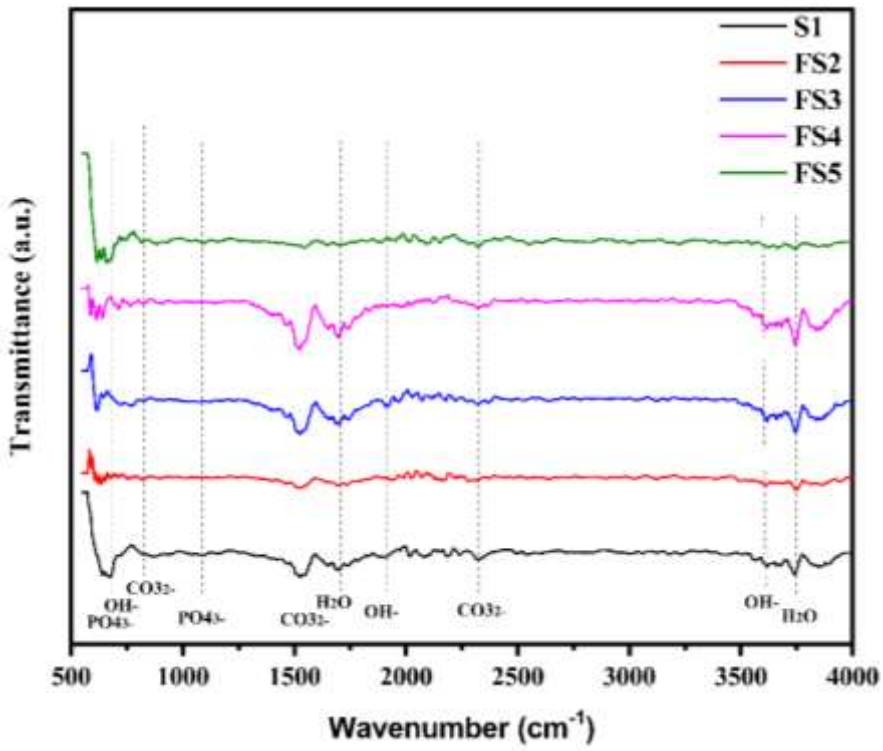

Figure 4-23 FTIR results for alkali treated hydroxyapatite coated samples for MoNbTaTiZr system

4.2.3 Electrochemical characterization

When the implant is placed in the body a chain of chemical reactions occurs on the implant surface. The chemical stability in the physiochemical environment is necessary to avoid the degradation of implant and release of toxic elements in the body which cause serious health related problems and results in failure of implant. To evaluate the chemical stability corrosion experiments were performed in the fluid containing same ion concentration as in human blood plasma. The experiments were performed at 37^0C, 7.4pH and three electrode assembly were used in which test sample used as working electrode, platinum wire as counter electrode and AG/AgCl as reference electrode. Electrochemical characterization of all the high entropy foam samples of understudy system was carried out and compare the results with dense alloy having no porosity. All the electrodes immersed in electrolyte for 3600 sec to stabilize the open circuit potential. After the stabilization of the system at equilibrium state the linear polarization resistance (LPR) experiment was performed from -10mV to +10mV VS OCP at scan rate of 0.166mV/sec.

Electrochemical impedance spectroscopy test were performed following the LPR to study corrosion resistance between the frequency range of 100K Hz to 10m Hz at OCP with a sinusoidal amplitude of 10mV. At the end, Potentiodynamic polarization test were performed from initial potential of -1500mV to final potential of 3000mV VS open circuit potential at the scan rate of 2mV/sec.

Figure 4-23(a) shows the OCP evolution with time for as cast and porous samples. With the increase in porosity, the potential value shift towards more negative potential observed for all the samples. S1, FS2, FS4, shows a little shift towards negative value before stabilization of potential whereas FS5 de-alloyed shows a large shift towards positive potential before stabilization of open circuit potential. However, all the samples show faster stability in simulated body environment by making a noble surface passive layer. After stabilizing the open circuit potential for 3600sec in simulated body fluid linear polarization resistance (LPR) was calculated. Figure 4-23(b) shows the graphical representation of LPR results. Polarization resistance and corrosion rate in (mpy) was calculated with E_{chem} analyst and given in table (2). FS5 show lowest corrosion rate of 0.2mpy with highest polarization resistance of 364 (k-ohms) and highest corrosion rate of 11.09mpy revealed by FS3 with lowest polarization resistance 6.67 (k-ohms). Overall, all the samples whether it is porous or non-porous demonstrate superior corrosion resistance without revealed any significant effect of porosity.

The Potentiodynamic polarization properties was studied with Tafel slopes after study linear polarization resistance. The parameters E_{corr} (corrosion potential), I_{corr} (corrosion current density), E_{pitt} (pitting potential) and Rp (polarization resistance) was calculated for both as cast and porous samples. Figure 4-23(c) shows that dense S1 shows nobler corrosion potential then the porous alloys. The E_{corr} value tends to decrease directly with increase in porosity as corrosion potential moves towards less noble behavior as porosity increases. All the alloys as cast and porous samples shows lower I_{corr} in simulated body fluid which shows the superior corrosion resistance of all the developed alloys in body environment conditions.

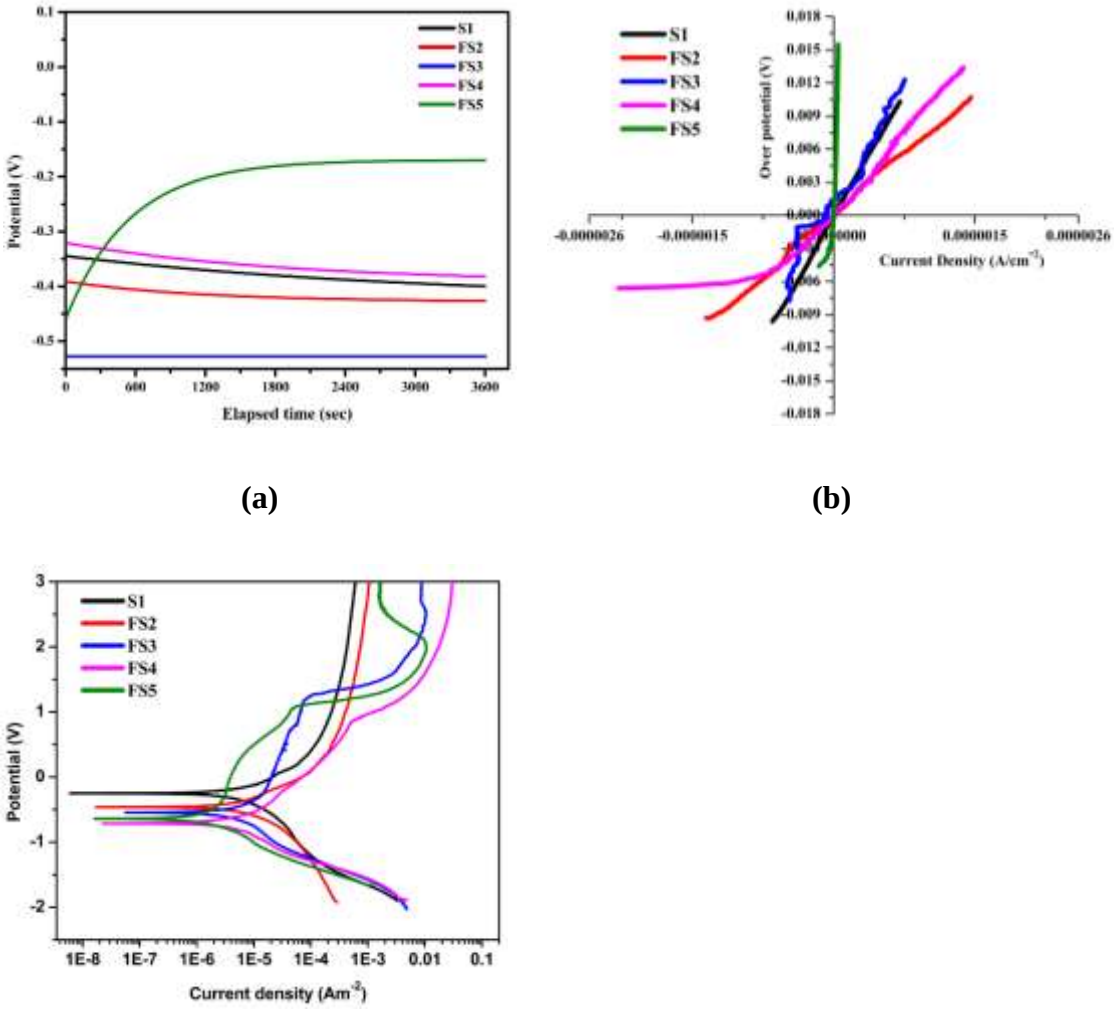

Figure 4-24Corrosion analysis results for MoNbTaTiZr high entropy foams in simulated body environment (a) Open circuit potential (b) Linear polarization resistance (c) Tafel plots

From the Figure 4-23(c) it is evident that as-cast alloy S1 and FS2 shows large stable passivation region without any sign of pitting whereas, all the other porous alloys show pitting at positive potentials. The pitting potential of porous alloys decreases with increase in porosity. The pitting of FS3 occurs at 1.25V, for FS4 at 0.83V and for FS5 at 1.05V, after that an abrupt increase in current density observed. βa & βc are anodic and cathodic constants which were calculated by extrapolating the Tafel slope and put values in butler-Volmer equation which becomes the Stern Geary equation near the Ecorr to calculate the

Rp. The table (2) shows the calculated values of Rp, all the alloys demonstrate superior corrosion resistance in simulated body environment required for biomedical applications.

Table 2 Corrosion analysis results for MoNbTaTiZr high entropy foams in simulated body environment

Sr.	**OCP**	**LPR**		**Potentiodynamic polarization**		
	Potential (mV)	**Rp(K-ohms)**	**Corrosion rate (mpy)**	**Ecorr (mv)**	**Icorr (A/cm^2)**	**E_{pitt} (V)**
S1	-398.4	15.28	7.38	-240	1.23×10^{-5}	---
FS2	-422	8.51	5.95	-460	8.80×10^{-5}	---
FS3	-530.9	6.67	11.09	-546	1.74×10^{-5}	1.24
FS4	-384.5	11.39	7.71	-716	1.34×10^{-5}	0.85
FS5	-159.8	364.1	0.2	-641	3.06×10^{-5}	1.09

The alloys did not follow specific pattern in terms of Icorr and Rp that can be explained as porous alloys till the porosity of 15% shows same corrosion behavior as dense samples[75], moreover limit localized corrosion observed after this range.

Conclusion

High entropy alloys were designed by Calphad software and fabricated by arc melting route. Yttrium was used as filler metal which then successfully removed by novel chemical dealloying process to form 3d porous structure. Structural evaluation proved that high entropy foams produced by this method have 3d porosity ranges from 4.1-18% with dual β-phase microstructure. Owing to this microstructure the developed high entropy foams shows a decreasing trend of elastic modulus, yield strength and Vickers hardness with increasing porosity. Therefore, it indicates the possibility to optimize the mechanical characteristics to prevent stress shielding effect. Surface characterization revealed that with increase in porosity surface roughness, surface area and hydrophilicity enhanced significantly, which then improve osseointegration. Alkali treatment of the high entropy foams were carried out which increase the surface energy and hydroxyapatite deposition during biomimetic coating, therefore promote uniform and compact hydroxyapatite coating. Corrosion analysis revealed that the developed high entropy foams demonstrate superior chemical stability in simulated body environment. Therefore, designed porous high entropy system is a promising candidate for orthopedic applications.

References

[1] Geetha, M., et al., *Ti based biomaterials, the ultimate choice for orthopaedic implants – A review.* Progress in Materials Science, (2009). **54**(3): p. 397-425.

[2] Abdel-Hady Gepreel, M. and M. Niinomi, *Biocompatibility of Ti-alloys for long-term implantation.* Journal of the Mechanical Behavior of Biomedical Materials, (2013). **20**: p. 407-415.

[3] Kurtz, S., et al., *Projections of primary and revision hip and knee arthroplasty in the United States from 2005 to 2030.* (2007). **89**(4): p. 780-785.

[4] Navarro, M., et al., *Biomaterials in orthopaedics.* Journal of the Royal Society, Interface, (2008). **5**(27): p. 1137-1158.

[5] Ogino, M., F. Ohuchi, and L.L. Hench, *Compositional dependence of the formation of calcium phosphate films on bioglass.* J Biomed Mater Res, (1980). **14**(1): p. 55-64.

[6] Schepers, E., et al., *Bioactive glass particulate material as a filler for bone lesions.* J Oral Rehabil, (1991). **18**(5): p. 439-52.

[7] Stanley, H.R., et al., *Using 45S5 bioglass cones as endosseous ridge maintenance implants to prevent alveolar ridge resorption: a 5-year evaluation.* Int J Oral Maxillofac Implants, (1997). **12**(1): p. 95-105.

[8] Hutmacher, D.W., *Scaffolds in tissue engineering bone and cartilage.* Biomaterials, (2000). **21**(24): p. 2529-2543.

[9] Sumner, D., et al., *Functional adaptation and ingrowth of bone vary as a function of hip implant stiffness.* (1998). **31**(10): p. 909-917.

[10] Rack, H.J. and J.I. Qazi, *Titanium alloys for biomedical applications.* Materials Science and Engineering: C, (2006). **26**(8): p. 1269-1277.

[11] Niinomi, M., M. Nakai, and J. Hieda, *Development of new metallic alloys for biomedical applications.* Acta Biomaterialia, (2012). **8**(11): p. 3888-3903.

[12] Li, Y., et al., *New Developments of Ti-Based Alloys for Biomedical Applications.* (2014). **7**(3): p. 1709-1800.

[13] Hao, Y.L., et al., *Aging response of the young's modulus and mechanical properties of Ti-29Nb-13Ta-4.6Zr for biomedical applications.* Metallurgical and Materials Transactions A, (2003). **34**(4): p. 1007-1012.

[14] Kuroda, D., et al., *Design and mechanical properties of new β type titanium alloys for implant materials.* Materials Science and Engineering: A, (1998). **243**(1): p. 244-249.

[15] Hao, Y.L., et al., *Super-elastic titanium alloy with unstable plastic deformation.* (2005). **87**(9): p. 091906.

[16] Kaya, M. and F. Yakuphanoğlu, *A study on microstructure of porous TiNbZr alloy produced as biomaterial.* Materialwissenschaft und Werkstofftechnik, (2019). **50**(6): p. 742-746.

[17] Bobyn, J.D., et al., *Producing and avoiding stress shielding. Laboratory and clinical observations of noncemented total hip arthroplasty.* (1992)(274): p. 79-96.

[18] Wen, C., et al., *Processing and mechanical properties of autogenous titanium implant materials.* (2002). **13**(4): p. 397-401.

[19] Greiner, C., S.M. Oppenheimer, and D.C. Dunand, *High strength, low stiffness, porous NiTi with superelastic properties.* Acta Biomaterialia, (2005). **1**(6): p. 705-716.

[20] Oppenheimer, S. and D. Dunand, *Solid-state foaming of Ti-6A1-4V by creep or superplastic expansion of argon-filled pores.* Acta Materialia - ACTA MATER, (2010). **58**: p. 4387-4397.

[21] Kirmanidou, Y., et al., *New Ti-Alloys and Surface Modifications to Improve the Mechanical Properties and the Biological Response to Orthopedic and Dental Implants: A Review.* BioMed Research International, (2016). **2016**: p. 2908570.

[22] Bose, S., S. Tarafder, and A. Bandyopadhyay, *7 - Hydroxyapatite coatings for metallic implants*, in *Hydroxyapatite (Hap) for Biomedical Applications*, M. Mucalo, Editor. (2015), Woodhead Publishing. p. 143-157.

[23] Milleret, V., et al., *Alkali treatment of microrough titanium surfaces affects macrophage/monocyte adhesion, platelet activation and architecture of blood clot formation.* Eur Cell Mater, (2011). **21**: p. 430-44; discussion 444.

[24] Niinomi, M., *Recent Research and Development in Titanium Alloys for Biomedical Applications and Healthcare Goods.* Science and Technology of Advanced Materials, (2003). **4**: p. 445-454.

[25] Cantor, B., et al., *Microstructural development in equiatomic multicomponent alloys.* Materials Science and Engineering: A, (2004). **375-377**: p. 213-218.

[26] Yeh, J.W., et al., *Nanostructured High-Entropy Alloys with Multiple Principal Elements: Novel Alloy Design Concepts and Outcomes.* Advanced Engineering Materials, (2004). **6**(5): p. 299-303.

[27] Tsai, M.-H. and J.-W. Yeh, *High-Entropy Alloys: A Critical Review.* Materials Research Letters, (2014). **2**(3): p. 107-123.

[28] Ye, Y.F., et al., *High-entropy alloy: challenges and prospects.* Materials Today, (2016). **19**(6): p. 349-362.

[29] Owen, L.R. and N.G. Jones, *Lattice distortions in high-entropy alloys.* Journal of Materials Research, (2018). **33**(19): p. 2954-2969.

[30] Kurtz, S.M., et al., *Future clinical and economic impact of revision total hip and knee arthroplasty.* J Bone Joint Surg Am, (2007). **89 Suppl 3**: p. 144-51.

[31] Karamian, E., et al., *An in vitro evaluation of novel NHA/zircon plasma coating on 316L stainless steel dental implant.* Progress in Natural Science: Materials International, (2014).

[32] Davidson, J. and F. Georgette, *State of the art materials for orthopedic prosthetic devices*. (1987): Society of Manufacturing Engineers.

[33] Okazaki, Y. and E. Gotoh, *Comparison of metal release from various metallic biomaterials in vitro.* Biomaterials, (2005). **26**(1): p. 11-21.

[34] Davis, J.R. *Handbook of Materials for Medical Devices*. (2003).

[35] Semlitsch, M. and H.G. Willert, *Properties of implant alloys for artificial hip joints.* Medical and Biological Engineering and Computing, (1980). **18**(4): p. 511-520.

[36] Al Jabbari, Y.S., *Physico-mechanical properties and prosthodontic applications of Co-Cr dental alloys: a review of the literature.* J Adv Prosthodont, (2014). **6**(2): p. 138-45.

[37] Sargeant, A. and T. Goswami, *Hip implants: Paper V. Physiological effects.* Materials & Design, (2006). **27**(4): p. 287-307.

[38] Majumdar, P., S.B. Singh, and M. Chakraborty, *The role of heat treatment on microstructure and mechanical properties of Ti-13Zr-13Nb alloy for biomedical load bearing applications.* J Mech Behav Biomed Mater, (2011). **4**(7): p. 1132-44.

[39] Zhang, L.C., et al., *Amorphization in mechanically alloyed (Ti, Zr, Nb)-(Cu, Ni)-Al equiatomic alloys.* Journal of Alloys and Compounds, (2007). **428**(1-2): p. 157-163.

[40] Elias, C., D. Fernandes, and R. Biasi, *Comparative study of compressive and fatigue strength of dental implants made of nanocrystalline Ti Hard and microcrystalline Ti G4.* Fatigue & Fracture of Engineering Materials & Structures, (2016). **40**.

[41] Sidambe, A.T., *Biocompatibility of Advanced Manufactured Titanium Implants-A Review.* Materials (Basel), (2014). **7**(12): p. 8168-8188.

[42] Ribeiro, A.L., et al., *Mechanical, physical, and chemical characterization of Ti-35Nb-5Zr and Ti-35Nb-10Zr casting alloys.* J Mater Sci Mater Med, (2009). **20**(8): p. 1629-36.

[43] Elias, C.N., et al., *Biomedical applications of titanium and its alloys.* JOM, (2008). **60**(3): p. 46-49.

[44] Chikumba, S. and V.V. Rao. *High entropy alloys: development and applications*. in *7th Int. Conf. Latest Trends Eng. Technol*. (2015).

[45] Jien-Wei, Y.J.A.C.S.M., *Recent progress in high entropy alloys.* (2006). **31**(6): p. 633-648.

[46] Liaw, P., J.-W. Yeh, and Y. Zhang, *High-entropy alloys: Fundamentals and applications*. (2016). 1-516.

[47] Geetha, M., et al., *Ti based biomaterials, the ultimate choice for orthopaedic implants–a review.* (2009). **54**(3): p. 397-425.

[48] Alvarado, J., et al., *Biomechanics of hip and knee prostheses.* (2003): p. 6-22.

[49] Niinomi, M., *Recent metallic materials for biomedical applications.* Metallurgical and Materials Transactions A, 2002. **33**(3): p. 477.

[50] Davis, E. and R.J.H.o.M.f.M.D.A.I.M.P. Davis, OH, *International A.* (2003).

[51] Facchini, L., et al., *Microstructure and mechanical properties of Ti-6Al-4V produced by electron beam melting of pre-alloyed powders.* Rapid Prototyping Journal, (2009). **15**: p. 171-178.

[52] Sidambe, A.T.J.M., *Biocompatibility of advanced manufactured titanium implants—A review.* (2014). **7**(12): p. 8168-8188.

[53] Lin, H.-I., et al., *Functional Studies of Anodic Oxidized β-Ti-28Nb-11Ta-8Zr Alloy for Mechanical, In-vitro and Antibacterial Capability.* Scientific Reports, (2018). **8**(1): p. 14253.

[54] Wang, S.-P. and J. Xu, *TiZrNbTaMo high-entropy alloy designed for orthopedic implants: As-cast microstructure and mechanical properties.* Materials Science and Engineering: C, (2017). **73**: p. 80-89.

[55] Dirras, G., et al., *Elastic and plastic properties of as-cast equimolar TiHfZrTaNb high-entropy alloy.* Materials Science and Engineering: A, (2016). **654**: p. 30-38.

[56] Senkov, O., et al., *Microstructure and room temperature properties of a high-entropy TaNbHfZrTi alloy.* (2011). **509**(20): p. 6043-6048.

[57] Yuan, Y., et al., *Formation, structure and properties of biocompatible TiZrHfNbTa high-entropy alloys.* Materials Research Letters, (2019). **7**(6): p. 225-231.

[58] Castro, D., et al., *An Overview of High-Entropy Alloys as Biomaterials.* (2021). **11**(4): p. 648.

[59] Motallebzadeh, A., et al., *Microstructural, mechanical and electrochemical characterization of TiZrTaHfNb and Ti1.5ZrTa0.5Hf0.5Nb0.5 refractory high-entropy alloys for biomedical applications.* Intermetallics, (2019). **113**: p. 106572.

[60] Shittu, J., et al., *Biocompatible High Entropy Alloys with Excellent Degradation Resistance in a Simulated Physiological Environment.* ACS Applied Bio Materials, (2020). **3**(12): p. 8890-8900.

[61] Akmal, M., H.-K. Park, and H.J. Ryu, *Plasma spheroidized MoNbTaTiZr high entropy alloy showing improved plasticity.* Materials Chemistry and Physics, (2021). **273**: p. 125060.

[62] Popescu, G., et al., *New TiZrNbTaFe high entropy alloy used for medical applications.* IOP Conference Series: Materials Science and Engineering, (2018). **400**: p. 022049.

[63] Kujala, S., et al., *Effect of porosity on the osteointegration and bone ingrowth of a weight-bearing nickel-titanium bone graft substitute.* Biomaterials, (2003). **24**(25): p. 4691-7.

[64] Zou, X., et al., *Bone ingrowth characteristics of porous tantalum and carbon fiber interbody devices: an experimental study in pigs.* Spine J, (2004). **4**(1): p. 99-105.

[65] Karageorgiou, V. and D. Kaplan, *Porosity of 3D biomaterial scaffolds and osteogenesis.* Biomaterials, (2005). **26**(27): p. 5474-91.

[66] Yong, L., M.E. Hoque, and I. Pashby, *Prediction of Patient-Specific Tissue Engineering Scaffolds for Optimal Design.* International Journal of Modeling and Optimization, (2013). **3**.

[67] Wen, C., et al., *Novel titanium foam for bone tissue engineering.* (2002). **17**(10): p. 2633-2639.

[68] Singh, R., et al., *Characterization of the structure and permeability of titanium foams for spinal fusion devices.* (2009). **5**(1): p. 477-487.

[69] Mullen, L., et al., *Selective Laser Melting: A regular unit cell approach for the manufacture of porous, titanium, bone in-growth constructs, suitable for orthopedic applications.* (2009). **89**(2): p. 325-334.

[70] Hollander, D.A., et al., *Structural, mechanical and in vitro characterization of individually structured Ti–6Al–4V produced by direct laser forming.* (2006). **27**(7): p. 955-963.

[71] Xie, C., et al., *Ti3Sn–NiTi Syntactic Foams with Extremely High Specific Strength and Damping Capacity Fabricated by Pressure Melt Infiltration.* ACS Applied Materials & Interfaces, (2019). **11**(31): p. 28043-28051.

[72] Zhao, Y., X. Tao, and X.J.M.S.T. Xue, *Manufacture and mechanical properties of metal matrix syntactic foams.* (2008). **4**: p. 2607-2615.

[73] Bharati, S., M.K. Sinha, and D.J.B.o.M.S. Basu, *Hydroxyapatite coating by biomimetic method on titanium alloy using concentrated SBF.* (2005). **28**: p. 617-621.

[74] Huynh, V., N.K. Ngo, and T.D. Golden, *Surface Activation and Pretreatments for Biocompatible Metals and Alloys Used in Biomedical Applications.* International Journal of Biomaterials, (2019). (**2019)**: p. 3806504.

[75] Fojt, J., L. Joska, and J. Malek, *Corrosion behaviour of porous Ti–39Nb alloy for biomedical applications.* Corrosion Science, (2013). **71**: p. 78–83.